Fermi Establishes Classical Novae as a Distinct Class of Gamma-Ray Sources

The Fermi-LAT Collaboration[*][†]

A classical nova results from runaway thermonuclear explosions on the surface of a white dwarf that accretes matter from a low-mass main-sequence stellar companion. In 2012 and 2013, three novae were detected in γ rays and stood in contrast to the first γ-ray detected nova V407 Cygni 2010, which belongs to a rare class of symbiotic binary systems. Despite likely differences in the compositions and masses of their white dwarf progenitors, the three classical novae are similarly characterized as soft spectrum transient γ-ray sources detected over $2-3$ week durations. The γ-ray detections point to unexpected high-energy particle acceleration processes linked to the mass ejection from thermonuclear explosions in an unanticipated class of Galactic γ-ray sources.

The Fermi-LAT [Large Area Telescope; (*1*)], launched in 2008, continuously scans the sky in γ rays, thus enabling searches for transient sources. When a nova explodes in a symbiotic binary system, the ejecta from the white dwarf surface expand within the circumstellar wind of the red giant companion and high-energy particles can be accelerated in a blast wave driven in the high-density environment (*2*) so that variable γ-ray emission can be produced, as was detected at >100 MeV energies by the LAT in V407 Cygni 2010 (V407 Cyg) (*3*). In a classical nova, by contrast, the ejecta quickly expand beyond the confines of the compact binary into a much lower density environment. High-energy particle acceleration could therefore be related to a bow shock driven by the ejecta in the interstellar medium, or to turbulence and eventually weaker internal shocks formed in the inhomogeneous ejecta itself. The contribution of such expanding nova shells to cosmic-ray acceleration had been considered (*4*), but no predictions have so far been made for >100 MeV γ-rays. The classical novae (or simply "novae" where appropriate) detected by the LAT with $12-20\sigma$ significances (Table 1, Fig. 1) – V959 Monocerotis 2012 (V959 Mon), V1324 Scorpii 2012 (V1324 Sco), and V339 Delphini 2013 (V339 Del) – were unanticipated. These observed γ rays have higher energies than nuclear line emission by

---

*All authors with their affiliations appear at the end of this paper. †To whom correspondence should be addressed. E-mail: Teddy.Cheung@nrl.navy.mil (C. C. Cheung); E-mail: Pierre.Jean@irap.omp.eu (P. Jean); E-mail: shore@df.unipi.it (S. N. Shore)

radioactive decay at $\sim$MeV energies that remain undetected in individual novae (*5*) and $\lesssim 0.1$ MeV emission detected in isolated cases (*6*).

V959 Mon was detected as a transient γ-ray source in June 2012 by the LAT while close ($\sim 20°$ separation) to the Sun (*7*) and then optically in August (*8*). Ultraviolet spectroscopy revealed an oxygen-neon nova (*9*), recognized as the class with the most massive white dwarfs ($\gtrsim 1.1$ $M_\odot$) with massive ($\gtrsim 8\ M_\odot$) progenitors [e.g., (*10*)]. The expected peak visual magnitude of $\sim$5 would have been observable with the naked eye $\sim$50 days earlier, when the γ-ray transient was detected (*9*). V339 Del (*11*) was detected in August 2013 in a LAT pointed observation triggered by its high optical brightness [4.3 mag at peak; (*12, 13*)]. Optical spectra of V339 Del suggest a carbon-oxygen nova (*14*), which are more common than the oxygen-neon types, with less massive white dwarfs evolved from $\lesssim 8\ M_\odot$ main-sequence progenitors. Optical brightening of V1324 Sco was detected in May 2012 (*15*) and found in LAT γ-ray data from June (*16*). Although the type for V1324 Sco is currently unclear, its optical spectroscopic evolution at early times (*15*) did not resemble oxygen-neon novae at similar stages. We take this to indicate it is likely a carbon-oxygen type.

The LAT data (*13*) for the three classical novae are discussed together with an updated analysis of the originally detected symbiotic nova V407 Cyg (*3*). The γ-ray light curves of all four systems (Fig. 2) are similar, with $2-3$ day long peaks occurring $3-5$ days after the initial LAT detections. The observed optical peak preceded the γ-ray peak by $\sim$2 days in V1324 Sco (*13, 17*) and $\sim$6 days in V339 Del (*12, 13*). Because the early optical light variations of the ejecta in novae are driven by line opacity changes in the ultraviolet during the expansion, the rise to peak optical brightness coincides with the maximum flux redistribution toward lower energies as the optically thick surface moves outward [see (*18*)]. The initial lack of detected γ rays could be because the ejecta are opaque and any >100 MeV emission produced are absorbed via photon-atom interactions, with γ rays appearing only later when the density drops and the ejecta become transparent. The three novae were detected in γ rays during a time of high X-ray and ultraviolet/optical opacity. Coincidentally, the few days' delay of the γ-ray peak relative to the optical peak was also observed in V407 Cyg, but this may instead signal interactions with its red giant companion (below).

In compact classical nova binaries, typical companion separations are $a \sim 10^{11}$ cm [$\sim 100\times$ larger in symbiotic systems; (*19*)] and expansion velocities v_{ej} at early times are many 100's to $\gtrsim 1000\ \mathrm{km\,s^{-1}}$. Thus the ejecta reach the companion on a timescale $t = 1000\,(a/10^{11}\ \mathrm{cm})$ $(v_{ej}/1000\ \mathrm{km\,s^{-1}})^{-1}$ s (i.e., of order an hour or less). Modeling of the optical line profiles indicates that the spatial distribution of the ejected gas is bipolar rather than spherical in all cases, with greater extension perpendicular to the orbital plane in V959 Mon (*9, 20, 21*). Also, narrow absorption and emission line structures seen in optical and ultraviolet line profiles later in the expansion may be evidence of hydrodynamical instabilities and multiple ejections that may lead to the formation of strong turbulence and internal shocks within the ejecta after the ignition of the thermonuclear runaway (*22*). A clue to the physical process that causes the γ-ray emission mechanism may be the similarity of the high-energy spectral characteristics of V1324

2

Sco, V959 Mon, and V339 Del. Their >100 MeV spectra are all soft, and can be fit with single power laws (the spectrum $N(E) \propto E^{-\Gamma}$ with the number N of photons with energy E) with photon indices $\Gamma = 2.1-2.3$, or exponentially cutoff power laws (the spectrum $N(E) \propto E^{-s}e^{-E/E_c}$, where E_c is the cutoff energy) – see (13), Table S1 and Fig. S1. The exponentially cutoff power law fits to the LAT data were preferred over the power law fits at the 3.8σ and 3.4σ level for V959 Mon and V339 Del, respectively, but provided an insignificant improvement (2.0σ) for V1324 Sco. Considering the uncertainties in the spectral fits, the three novae are similarly characterized by slopes $s = 1.7-1.8$, $E_c \sim 1-4$ GeV, and observed emission up to $\sim6-10$ GeV. The total durations of the observed γ rays were also similar, being detected for $17-27$ days at $>2\sigma$ statistical significances in daily bins (Fig. 2, Table 1). Because the LAT-observed properties are similar, it is likely that the γ-ray emission of these classical novae has a similar origin, involving interactions of the accelerated high-energy protons (hadronic scenario) or electrons (leptonic scenario) within the ejecta.

In the hadronic scenario, high-energy protons that interact with nuclei produce neutral pions (π^0), which decay into two γ rays. For a representative hadronic model, we assume an exponentially cutoff power law distribution of protons in the form, $N_p(p_p) = N_{p,0}(p_p c)^{-s_p}e^{-W_p/E_{cp}}$ (proton/GeV), where p_p and W_p are the momentum and the kinetic energy of protons, respectively, $N_{p,0}$ the normalization, s_p the slope, and E_{cp} the cutoff energy. We fitted E_{cp} and s_p with the LAT spectra to obtain the best-fit π^0 models (Fig. 3). The lower limits to the cutoff energies ($\sim3-30$ GeV) suggest proton acceleration up to near-TeV energies. The slopes of the best-fit models of the proton spectrum have large statistical uncertainties (~ 0.8) but interestingly are compatible with a value of 2 expected in the first order Fermi acceleration process. To match the observed γ-ray variability timescale in such a process, a magnetic field $B > 10^{-3}$ Gauss is required in a strong shock with $v_{ej} = 2000$ km s^{-1} to accelerate particles to $> 1(10)$ GeV energies in $\sim 0.2(2)$ days. Formally, the updated best-fit proton spectrum for the symbiotic nova V407 Cyg [cf., (3)] is parameterized by $s_p = 1.4^{+0.3}_{-0.4}$ GeV, but slopes of 2 – 2.2 are also viable at the 90% confidence level with $E_{cp} = 10^{+1.0}_{-0.7}$ GeV [(13), Fig. S3]. Lower-confidence fits were also obtained for V959 Mon and V339 Del but conversely with smaller slopes and lower cutoff energies [(13), Fig. S3]. Assuming that the γ-ray flux is due to the interactions of high-energy protons with the nuclei in the ejecta, the best-fit parameters allow us to estimate the total energy in high-energy protons of $\sim(3-17) \times10^{42}$ ergs and to derive conversion efficiencies (i.e., the ratio of the total energy in high-energy protons to the kinetic energy of the ejecta) ranging from $\sim0.1-3.7\%$ for the classical novae and 6.6% for V407 Cyg.

In the leptonic case, accelerated electrons produce γ rays through a combination of inverse Compton scattering with low-energy photons and bremsstrahlung with atoms in the vicinity of the nova. For a leptonic model, we adopted a similar functional form for the distribution of the kinetic energy of high-energy electrons (W_e) in the form $N_e(W_e) = N_{e,0}W_e^{-s_e}e^{-W_e/E_{ce}}$ (electron/GeV), and fitted the normalization $N_{e,0}$, slope s_e, and cutoff energy E_{ce} to the LAT data for each nova (Fig. 3). The γ-ray luminosity of the calculated bremsstrahlung emission is <20% of the total γ-ray luminosity for all the novae (13). The best-fit parameters of the

3

high-energy electron spectra for the three classical novae are similar within their confidence regions (*13*), with E_{ce} constrained to lie between 2 and 30 GeV, and poorly constrained slopes. These models are statistically indistinguishable from the π^0 model. As in the hadronic model, the spectral parameters of the classical novae differ from those for V407 Cyg (mainly due to the lowest-energy $\sim 200-300$ MeV bin detected in its LAT spectrum) where the best-fit slope is negative (i.e., a positive index of the power law) and $E_{ce} = 1.78 \pm 0.05$ GeV. The best-fit parameters for the leptonic scenario, where high-energy electrons interact primarily with the photons emitted by the nova photosphere (*23*), lead to total energies of $\sim(6-13) \times 10^{41}$ ergs in high-energy electrons and conversion efficiencies of $\sim 0.1 - 0.3\%$ for the classical novae and 0.6% for the symbiotic system.

Detection of classical novae in γ rays was deemed unlikely in the past (*3*). The only nova previously detected in γ rays, the aforementioned V407 Cyg, was a rare symbiotic and likely recurrent [only 10 recurrent novae are known, of which 4 are symbiotic types; (*24*)]. In the symbiotic novae, conditions are conducive for high-energy particle acceleration as the portion of the ejecta moving into the wind in the direction of the dense medium provided by the red giant companion decelerates within a few days. The γ-rays peak early, when the efficiency for hadron and lepton acceleration is presumably favorable, with the red giant wind playing a key role in the γ-ray production [see (*2, 23*)]. In contrast, the main-sequence star companions in the classical novae do not provide similarly dense target material, hence it is likely that other dissipative processes are involved in particle acceleration and generation of the observed γ rays.

Because the γ-ray properties of the novae detected so far by the Fermi-LAT appear similar to one another, and their underlying properties are unremarkable, it appears all novae can be considered to be candidate γ-ray emitters. Their detection by the LAT may imply close proximity and that other optical novae not yet detected with the LAT [e.g., (*25*)] are more distant and have fainter optical peaks [without considering extinction uncertainties (*26*)]. Indeed, all the LAT-detected novae have estimated distances of $\lesssim 4-5$ kpc (Table 1). Despite systematic uncertainties in the adopted distances, it is interesting that the inferred mean γ-ray luminosities and total emitted energies of the novae span a small range $\sim(3-4)\times10^{35}$ ergs s^{-1} and $\sim(6-7)\times10^{41}$ ergs, respectively, except for the $\sim2\times$ greater values for V1324 Sco whose distance is highly uncertain.

The rate of novae in the Milky Way is highly uncertain, but considering a plausible range of $\sim20-50$ per year (*27*) and reasonable spatial distributions in the Galactic bulge and disk (*28*), our estimate is $1-4$ per year at $\lesssim 4-5$ kpc distances. The γ-ray detection rate of novae averages roughly to once per year over the timespan of these observations (~5 years), consistent with the lower end of this extrapolation.

Although the γ-ray properties of the LAT-detected novae are similar, we emphasize the small and subtle differences that imply different emission mechanisms, e.g., the spectral shape of V407 Cyg compared to the three classical novae as well as the apparent higher energy extension of the V1324 Sco spectrum. Among the classical novae detected so far, they also appear different optically. The γ-ray emission mechanism and high-energy particle acceleration pro-

cesses associated with the novae could depend on the particular system properties that remain to be investigated, such as the white dwarf mass, which determines the explosion energetics (ejected mass, expansion velocity), and the mass transfer dictated by the companion mass and separation.

References and Notes

1. W. B. Atwood *et al.*, *Astrophys. J.* **697**, 1071 (2009).

2. V. Tatischeff, M. Hernanz, *Astrophys. J. Lett.* **663**, L101 (2007).

3. A. A. Abdo *et al.*, *Science* **329**, 817 (2010).

4. V. L. Ginzburg, S. I. Syrovatskii, The Origin of Cosmic Rays (Macmillan, New York, 1964) pp. 200-202.

5. M. Hernanz, in Classical Novae, 2nd Ed., M. F. Bode, A. Evans, Eds. (Cambridge Univ. Press, Cambridge, 2008) p. 252.

6. D. Takei *et al.*, *Astrophys. J. Lett.* **697**, L54 (2009).

7. C. C. Cheung, E. Hays, T. Venters, D. Donato, R. H. D. Corbet, Fermi-LAT collaboration, *The Astronomer's Telegram* **4224**, 1 (2012).

8. S. Fujikawa, International Astronomical Union Central Bureau for Astronomical Telegrams, reported by M. Soma, no. 3202 (2012).

9. S. N. Shore *et al.*, *Astron. Astrophys.* **553**, 123 (2013).

10. S. Starrfield, W. M. Sparks, J. W. Truran, *Astrophys. J. Lett.* **303**, L5 (1986).

11. K. Itagaki, International Astronomical Union Central Bureau for Astronomical Telegrams, reported by S. Nakano, no. 3628 (2013).

12. E. Hays, T. Cheung, S. Ciprini, Fermi-LAT collaboration, *The Astronomer's Telegram* **5302**, 1 (2013).

13. Supplementary materials are available on *Science* Online.

14. S. N. Shore, P. Skoda, P. Rutsch, *The Astronomer's Telegram* **5282**, 1 (2013).

15. R. M. Wagner *et al.*, *The Astronomer's Telegram* **4157**, 1 (2012).

16. C. C. Cheung, T. Glanzman, A. B. Hill, Fermi-LAT collaboration, *The Astronomer's Telegram* **4284**, 1 (2012).

17. A. B. Hill, Fermi-LAT collaboration, in 4th Fermi Symposium, Monterey CA, eConf C121028, 112 (2012).

18. S. N. Shore, *Bull. Astron. Soc. India* **40**, 185 (2012).

19. U. Munari, R. Margoni, R. Stagni, *Mon. Not. R. Astron. Soc.* **242**, 653 (1990).

20. V. A. R. M. Ribeiro, U. Munari, P. Valisa, *Astrophys. J.* **768**, 49 (2013).

21. G. H. Herbig, J. I. Smak, *Acta Astron.* **42**, 17 (1992).

22. J. Casanova, J. José, E. García-Berro, S. N. Shore, A. C. Calder, *Nature* **478**, 490 (2011).

23. P. Martin, G. Dubus, *Astron. Astrophys.* **551**, A37 (2013).

24. B. E. Schaefer, *Astrophys. J. Suppl. Ser.*, **187**, 275 (2010).

25. C. C. Cheung, Fermi-LAT collaboration, in 4th Fermi Symposium, Monterey CA, eConf C121028, 106 (2012).

26. K. Mukai, `http://asd.gsfc.nasa.gov/Koji.Mukai/novae/novae.html`, September 4, 2013 version

27. A. W. Shafter, *Astrophys. J.* **487**, 226 (1997).

28. P. Jean, M. Hernanz, J. Gómez-Gomar, J. José, *Mon. Not. R. Astron. Soc.* **319**, 350 (2000).

29. M. M. Kasliwal *et al.*, *Astrophys. J.* **735**, 94 (2011).

30. S. N. Shore, *The Astronomer's Telegram* **5410**, 1 (2013).

31. P. L. Nolan *et al.*, *Astrophys. J. Suppl. Ser.* **199**, 31 (2012).

32. M. Ackermann *et al.*, *Astrophys. J. Suppl. Ser.* **203**, 4 (2012).

33. J. R. Mattox *et al.*, *Astrophys. J.* **461**, 396 (1996).

34. T. Kamae, N. Karlsson, T. Mizuno, T. Abe, T. Koi, *Astrophys. J.* **647**, 692 (2006).

35. M. Mori, *Astropart. Phys.* **31**, 341 (2009).

36. J. C. Houck, G. E. Allen, *Astrophys. J. Suppl. Ser.* **167**, 26 (2006).

37. C. D. Dermer, G. Powale, *Astron. Astrophys.*, **553**, A34 (2013).

38. G. R. Blumenthal, R. G. Gould, *Rev. Mod. Phys.* **42**, 237 (1970).

39. R. Greimel, J. Drew, D. Steeghs, M. Barlow, *The Astronomer's Telegram* **4365**, 1 (2012).

40. S. van den Bergh, P. F. Younger, *Astron. Astrophys. Suppl.* **70**, 125 (1987)

41. M. della Valle, M. Livio, *Astrophys. J.* **452**, 704 (1995).

42. M. J. Darnley, M. F. Bode, R. J. Smith, A. Evans, *The Astronomer's Telegram* **5279**, 1 (2013).

43. T. Tomov, K. Ilkiewicz, E. Swierczynski, M. Belcheva, D. Dimitrov, *The Astronomer's Telegram* **5288**, 1 (2013).

44. J. Wren, W. T. Vestrand, P. Wozniak, H. Davis, *The Astronomer's Telegram* **5316**, 1 (2013).

45. U. Munari, A. Henden, *Information Bulletin on Variable Stars* **6087**, 1 (2013).

46. N. R. Deacon *et al.*, *Astron. Astrophys.* **563**, A129 (2014).

47. U. Munari, P. Valisa, A. Milani, G. Cetrulo, *The Astronomer's Telegram* **5297**, 1 (2013).

48. S. N. Shore *et al.*, *The Astronomer's Telegram* **5409**, 1 (2013).

49. We acknowledge with thanks the variable star observations from the AAVSO International Database contributed by observers worldwide and used in this research, and the dedicated observers of the Astronomical Ring for Access to Spectroscopy (ARAS) group for their tireless and selfless efforts.

| Nova	V407 Cyg 2010	V1324 Sco 2012	V959 Mon 2012	V339 Del 2013
Distance (kpc)	2.7	4.5	3.6	4.2
Peak magnitude	6.9	10.0	5*	4.3
Peak date	2010 Mar 10.80	2012 Jun 19.96	...	2013 Aug 16.50
Optical RA, Decl.	315.5409°, +45.7758°	267.7246°, –32.6224°	99.9108°, +5.8980°	305.8792°, +20.7681°
Optical l, b	86.9826°, –0.4820°	357.4255°, –2.8723°	206.3406°, +0.0754°	62.2003°, –9.4234°
LAT RA, Decl.	315.57°, +45.75°	267.72°, –32.69°	99.98°, +5.86°	305.91°, +20.78°
Optical-LAT offset	0.03°	0.07°	0.08°	0.03°
LAT error radius (95%)	0.08°	0.09°	0.18°	0.12°
t_s (date)	2010 Mar 10	2012 Jun 15	2012 Jun 19	2013 Aug 16
t_s (MJD)	55265	56093	56097	56520
Duration (days)	22	17	22	27
L_γ (10^{35} erg s^{-1})	3.2	8.6	3.7	2.6
Total energy (10^{41} erg)	6.1	13	7.1	6.0

Table 1 – Summary of the Four Novae. Tabulated are optical peak magnitudes and adopted distances from (*19*) for V407 Cyg, estimate of ∼4−5 kpc V1324 Sco based on the maximum magnitude rate of decline relation (*17*) notwithstanding the large uncertainties in this method (*29*), (*9*) for V959 Mon (scaled from V1974 Cyg 1992), and (*30*) for V339 Del (scaled from OS Andromedae 1986), and observed dates of the optical peaks (unfiltered from (*3*), V-band, adopted, and visual magnitudes, respectively). Positions in J2000.0 equinox (right ascension, RA; declination, Decl.), Galactic longitude (l) and latitude (b), 95% confidence localization error radius, and offset between the LAT and optical positions in units of degrees. Adopted start dates t_s (*13*) are given in Gregorian Dates and Modified Julian Days (MJD). The γ-ray luminosities L_γ and total emitted energies were estimated with the average fluxes from the power law fits of the >100 MeV LAT spectra integrated up to 10 GeV and durations from t_s up to the last > 2σ daily bin LAT detection. For V339 Del, the γ rays were detected for 25 days in 1-day bins (Fig. 2), but there was a hint of a detection two days earlier on the day of the optical peak in 0.5-day binned data (*13*), leading to a 27 day duration.

*Note that for V959 Mon the optical peak magnitude of 9.4 (unfiltered) was observed ∼50 days after the initial γ-ray detection, and we adopted an inferred peak of 5 magnitude (*9*).
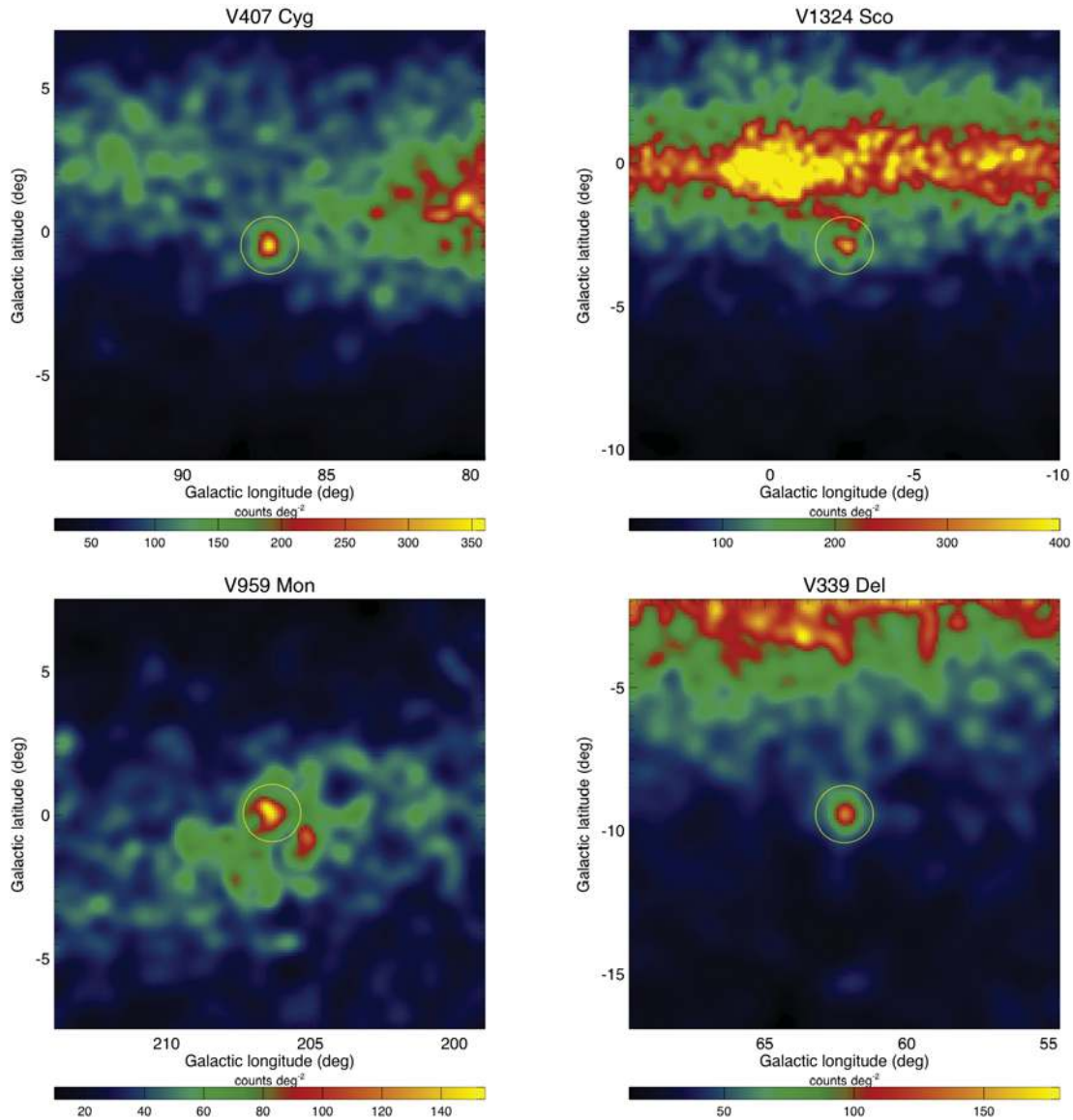
Fig. 1. Fermi-LAT >100 MeV γ-ray counts maps of the four novae in Galactic coordinates centered on the optical positions over the full $17-27$ day durations. The maps used $0.1° \times 0.1°$ pixels and were adaptively smoothed with a minimum number of $25-50$ counts per kernel. Each nova (located at the centers of the yellow circles with $1°$ radius which is the approximate LAT 95% containment at 1 GeV) is observed near the bright diffuse γ-ray emission in the Galactic plane, with V959 Mon in particular observed directly through the plane ($0°$ latitude).

9
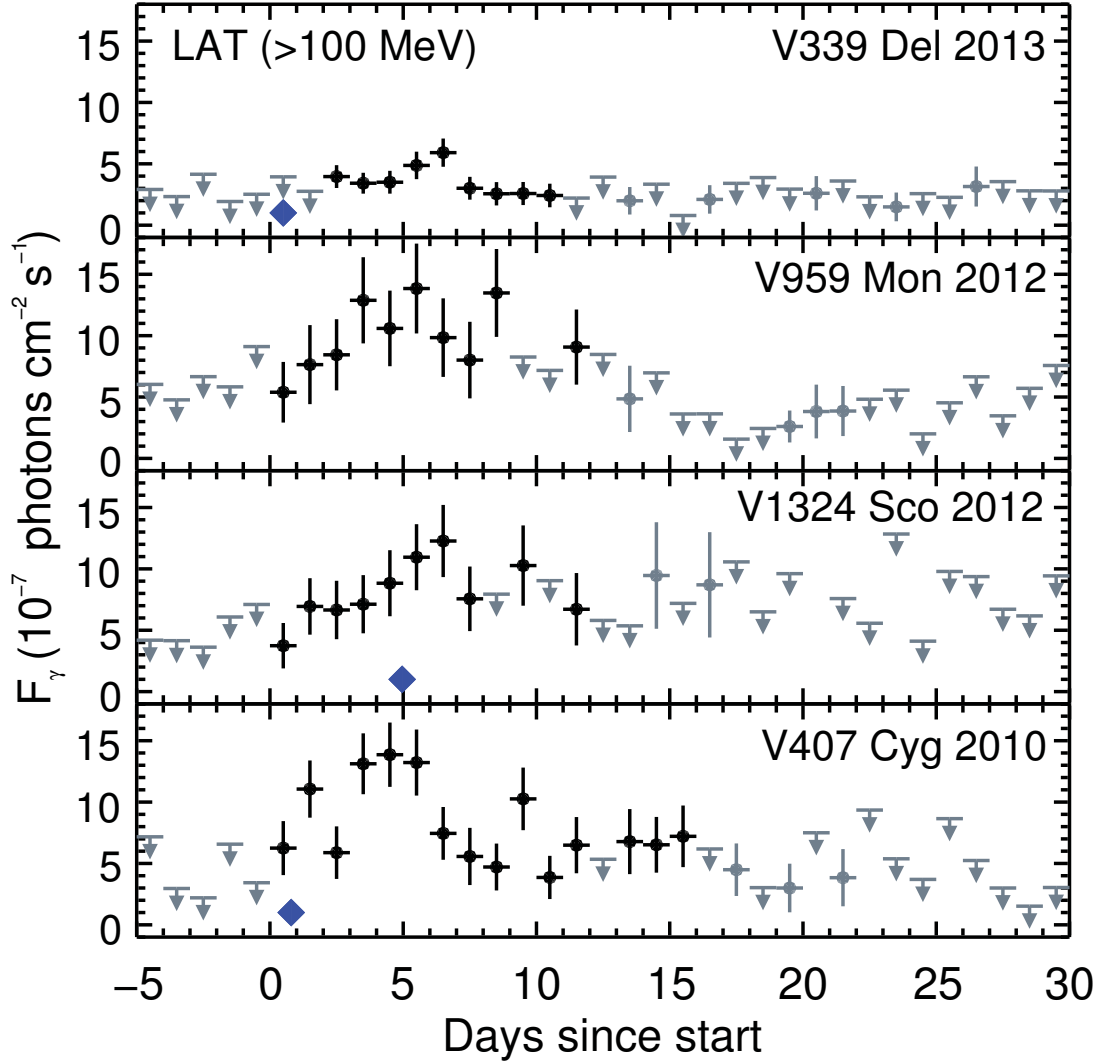
Fig. 2. Fermi-LAT 1-day binned light curves of the four γ-ray detected novae. Vertical bars indicate 1σ uncertainties for data points with $> 3\sigma$ (black) and $2\text{-}3\sigma$ (gray) significances, otherwise, 2σ upper limits are indicated with gray arrows. Start times t_{s} (from top to bottom panels) of 2013 August 16, 2012 June 19, 2012 June 15, and 2010 March 10 were defined as the day of the first γ-ray detection. In V339 Del, there was a 2.4σ detection in 0.5-day binned data beginning August 16.5 (*13*), the epoch of the optical peak (blue diamond in each panel).
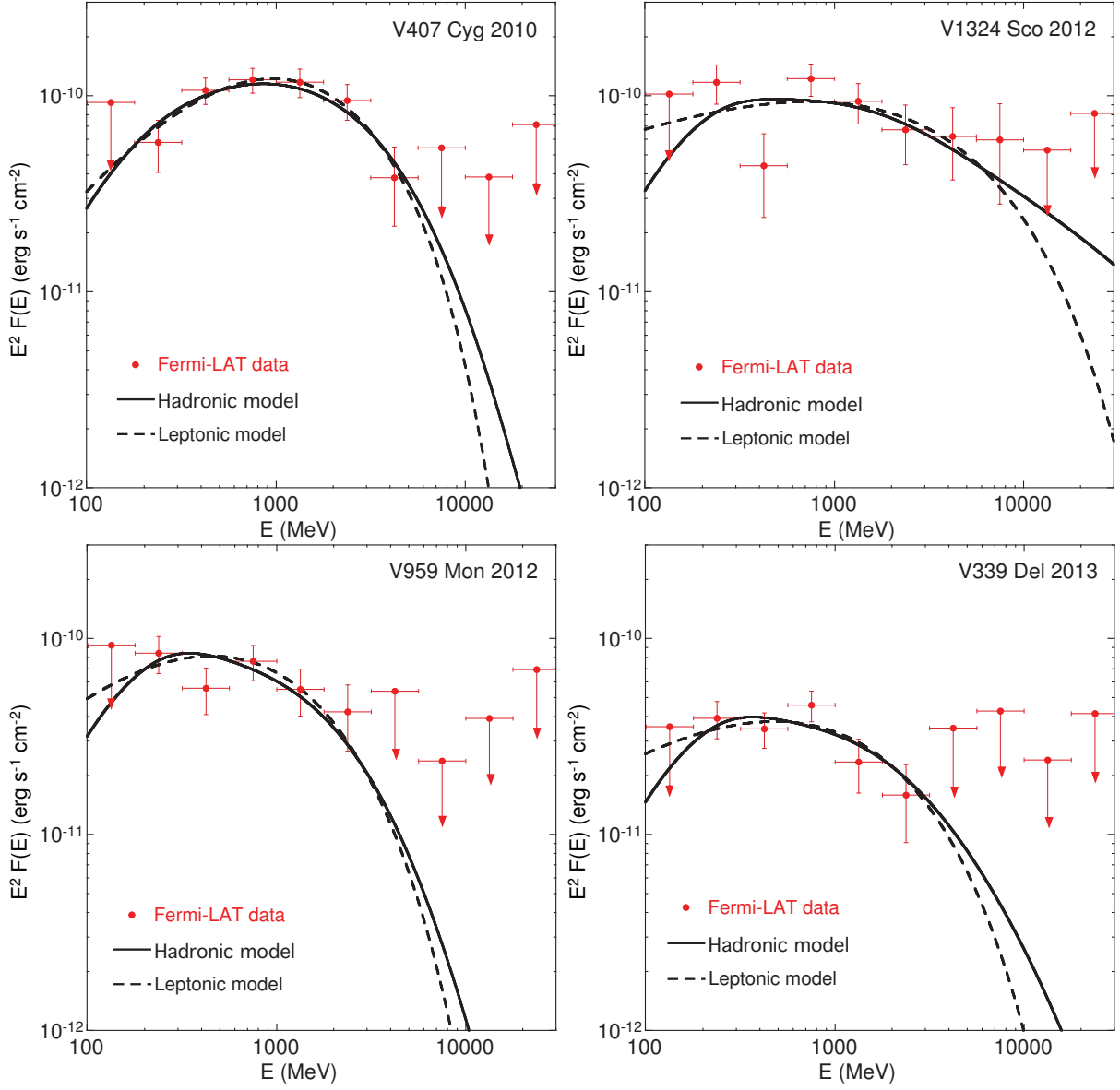
Fig. 3. Fermi-LAT >100 MeV average γ-ray spectra of the four novae over the full $17-27$ day durations. Vertical bars indicate 1σ uncertainties for data points with significances $> 2\sigma$; otherwise, arrows indicate 2σ limits. The best-fit hadronic and leptonic model curves are overlaid.

11

Supplementary Materials for

Fermi Establishes Classical Novae as a Distinct Class of Gamma-Ray Sources

The Fermi-LAT Collaboration[1]

†correspondence to: Teddy.Cheung@nrl.navy.mil (C. C. Cheung), Pierre.Jean@irap.omp.eu (P. Jean), shore@df.unipi.it (S. N. Shore)

This PDF file includes:

---

[1]All authors with their affiliations appear at the end of this paper.

Materials and Methods

S1. Fermi-LAT Observations and Analysis

The Fermi Large Area Telescope (LAT) (*1*) is sensitive to γ rays from 20 MeV to >300 GeV. It features a large instantaneous field of view (2.4 steradian) and began operations in 2008 August nominally in survey mode where an all-sky image is obtained every two orbits ($\sim$3 hrs). Three of the novae (V407 Cyg, V1324 Sco, V959 Mon) were detected over the course of the LAT all-sky survey. For V407 Cyg, our analysis here updates that originally published (*3*) with the γ-ray event selection cuts and associated instrument response functions to match those used for the new cases. V1324 Sco in particular was found in the field of a source being monitored for other reasons [see (*17*)] and was detected in γ rays as early as June 15 (just four days earlier than V959 Mon). Its positional and temporal coincidence with V1324 Sco [MOA 2012-BLG-320, (*15*)] was noticed later (*16*). V339 Del was the subject of a Fermi target-of-opportunity (ToO) pointing observation triggered by the bright optical discovery (*11*). The ToO began 2013 August 16.5 UT, the day of the optical peak (Section S3). The V339 Del ToO lasted for six days and resulted in $\sim$3$\times$ greater exposure with the LAT than would have been possible in all-sky survey mode, leading to improved statistics that were especially useful because of the relative faintness of the nova (below).

For the LAT analysis, we selected 100 MeV to 100 GeV events within regions of interest (ROI) of 15° radius centered on each nova optical position (Table 1) using the Pass 7 data and P7SOURCE_V6 instrument response functions (IRFs)[2]. Data were selected with a rocking angle cut of 52° and maximum zenith angle of 100° in order to minimize contamination from Earth limb photons, using gtmktime with the filter (#3) recommended for the combination of sky survey and ToO observations[3]. To model the diffuse γ-ray background and nearby γ ray sources we utilized the isotropic and Galactic diffuse emission templates[4] and included all sources from the 2nd Fermi Gamma-ray LAT [2FGL, (*31*)] catalog within the ROI. The analysis used version v9r27p1 of the Fermi science tools assuming a point source for each target.

Uncertainties shown in the plots are statistical. Two major sources of systematic errors on the results are the uncertainties in the LAT effective area and the modeling of interstellar emission, since all these novae lie close to the Galactic plane. The uncertainties in the effective area for the IRFs we use are evaluated as 10% at 100 MeV, 5% at 560 MeV, and 10% above 10 GeV, linearly varying with the logarithm of energy between those values (*32*). In all cases, the statistical uncertainties exceed these values. The uncertainty due to the interstellar emission model does not affect the light curves but would enlarge the uncertainties on the spectral

---

[2]Cross-checks with the newer Pass 7 reprocessed data and response functions produced results consistent within the quoted uncertainties.

[3]http://fermi.gsfc.nasa.gov/ssc/data/analysis/documentation/Cicerone/
Cicerone_Likelihood/Exposure.html

[4]Files iso_p7v6source.txt and gal_2yearp7v6_v0.fits, respectively.

measurements.

Light curves and Durations

To determine the interval and duration over which γ-ray emission was detected for each nova, we generated LAT light curves using a binned `gtlike` analysis in daily bins centered at fiducial start times t_s set to the first reported LAT detection for V407 Cyg (*3*), V1324 Sco (*16*), and V959 Mon (*7*). For V339 Del, the first LAT detection in 1-day bins was on August 18 (see Sec. S3), but there was indication for a marginal detection (see below) in 0.5 day bins when the optical peak was observed two days earlier; thus t_s was set to the latter in this case. The full interval studied for each nova was 106 days, i.e., $t_s \pm 53$ days (to gauge the effect of varying exposure over two precession periods of the spacecraft orbit), except for V339 Del, for which 2013 September 30 (MJD 56565) was the last day of data used (for $t_s = 56520$; this is t_s $-61/+45$ days). The start times defined in this way do not necessarily coincide with the optical discovery date, which is in contrast in some cases to the convention often adopted in the nova literature. We chose to define the start times in this way because the γ-ray emission is often detected at or near the optical peaks and these seem to be the relevant time windows to utilize for the light curve comparisons. For V407 Cyg, the first daily bin γ-ray detection coincided with the apparent optical peak observed on the discovery date, although there was an uncertainty in the optical peak epoch of up to three days due to an observing gap. In the case of V1324 Sco (*17*), the optical discovery date of May 22.80 UT (*15*) was 23 days before the first LAT detection, making the former an impractical choice of a start time for this work. For V339 Del (*12*), the discovery date was two days before the optical peak when the first LAT detection occurred in 0.5-day binned data (below), but a further two days before the first daily LAT detection.

For all light curves, we left the normalization of the isotropic diffuse spectrum as a free parameter in each time bin while the Galactic normalization was initially fit over the full 106-day interval, then fixed at the average fitted value in the shorter time-bins. All 2FGL sources within each ROI were included in the model using their cataloged spectral parameters (*31*). For the 2FGL sources within 5° of the novae positions known to be variable [according to (*31*)], the flux normalizations were initially fit over each 106-day interval. The newly fitted fluxes were assumed for the variable sources if significantly detected with test statistic (*33*) $TS > 10$, otherwise, the 2FGL fluxes were used in the subsequent 1-day binned analysis. We assumed a power-law (PL; the spectrum $N(E) \propto E^{-\Gamma}$) spectral model for point sources fit at the optical nova positions. The 1-day binned data were initially fit with free normalization and photon index Γ. We found no statistically significant variations in the index from the average values of the most significant detections with $TS > 9$, $\Gamma = 2.2$ for V407 Cyg ($N = 15$ bins) and V339 Del ($N = 9$). We similarly found no significant variations from the average daily values $\Gamma = 2.2$ for V1324 Sco ($N = 7$) and 2.4 for V959 Mon ($N = 6$) considering instead a larger $TS > 15$ threshold because of the brighter Galactic diffuse background in these cases. We then fixed the PL spectral slopes and regenerated the light curves to determine durations over which

to sum the data to fit average spectra (below). The final daily light curves presented in Fig. 1 assumed $\Gamma = 2.2$ (V407 Cyg, V1324 Sco) and 2.3 (V959 Mon, V339 Del), with the latter taken to match the values fitted below over the total intervals; V407 Cyg was not adjusted because of the significant spectral curvature detected.

Considering a $TS > 4$ threshold[5] for detections rather than upper limits in the 1-day binned light curves (Fig. 2; tabulated in Table S2), the resultant observed durations of detectable γ-ray emission were $2-3$ weeks for all sources. More precisely, the observed range was $17-22$ days for the first three novae. For V339 Del, γ rays were detected for 25 days beginning 1.5 days after the optical peak observed on August 16.5. Note however, that the ToO observation commenced also on August 16.5; thus we generated a LAT light curve with 0.5 day bins and found $TS = 0$ for the earlier bin and $TS = 5.6$ with >100 MeV flux = $(2.5 \pm 1.3) \times 10^{-7}$photons cm^{-2} s^{-1} for the latter half which benefitted from the increased exposure from the ToO. We therefore defined the duration for V339 Del to be 27 days. Because the varying exposures over the timescales of many weeks for the LAT observations may complicate statements about the detectability of each nova at both early and late times, this may affect our measured γ-ray durations, hence estimates of the total energy emitted in γ rays. As a final note, applying the same $TS > 4$ threshold to the original LAT analysis for V407 Cyg results in a γ-ray duration of 18 days [(3), Table S1 therein], and is shorter than the 22 days we found in our reanalysis (due to an increase in TS of two bins from ~$1-2$ to 4; Table S2).

Positions

To obtain the most precise source positions with the LAT, we performed an unbinned `gtlike` analysis assuming a single PL model over the γ-ray active durations defined in the 1-day binned analysis. The resultant formal integrated detection significances were $12-20\sigma$; the corresponding sky counts maps are shown in Fig. 1. We then ran `gtfindsrc` and obtained 95% confidence error radii of $0.068° - 0.16°$ (statistical only), meaning all sources were well localized. In the values reported in Table 1, we included a 10% allowance for systematic uncertainties as applied for the 2FGL catalog (31). This is a conservative estimate because the time intervals analyzed here are considerably shorter, and the statistical uncertainties correspondingly larger, than for the 2FGL catalog. The stellar counterparts for each nova were within the obtained LAT error circles, being within the 68% confidence region for three cases, and within 95% for V1324 Sco which may suffer from larger systematic uncertainty due to large gradients in the bright diffuse γ-ray emission in the Galactic bulge.

Spectra

The LAT spectra of the novae were extracted in 12 logarithmic energy bins from 100 MeV to 100 GeV. The fit results for single PL and exponentially cutoff power-law (EPL; the spectrum

---

[5]The source significance is $\sim \sqrt{TS}$ assuming one degree of freedom.

$N(E) \propto E^{-s}e^{-E/E_c}$) models are plotted over the LAT data in Fig. S1 and summarized in Table S1. With the extra degree of freedom in the EPL model versus the single PL, the fits were improved with significances of 3.4σ for V339 Del and 3.8σ for V959 Mon, but only marginally at 2.0σ for V1324 Sco. The new analysis of V407 Cyg yielded a 6.4σ significance of the spectral curvature, confirming the original analysis in (3). Interestingly, we also see marginal evidence in all four novae of a downturn of the LAT spectrum at the low energy end with no significant emission in the lowest energy $(100-178 \text{ MeV})$ spectral point in each case. The 95% confidence upper limits derived in this energy bin are at, or just below, the PL model for all four examples. Along with the statistical uncertainties, systematic uncertainties in the Galactic diffuse γ-ray emission limit the spectral shape measurements to varying degrees depending on the location of each nova studied. Because V1324 Sco is seen against the Galactic bulge and has the brightest diffuse background, the spectral shape was more difficult to measure and the cutoff energy in the EPL fit was not well constrained. Regardless, the inferred cutoff energies are $1-4$ GeV with indices $= 1.2-1.8$ in the EPL model fits.

Search for Spectral Variability

In order to check whether the spectral characteristics changed during the γ-ray flares, each data set was split into the time intervals specified in Table S1. The same method as the one presented previously for the full duration datasets was used to analyze both split sets of data. The resultant best-fit parameters are tabulated in Table S1 and the spectral energy distributions are presented in Fig. S2. For each nova, the first intervals (a) were six days long beginning at t_s, and resulted in comparable TS values ($\sim1-1.5\times$ larger) than those in the second intervals (b) which range from 11 to 21 days long. Although the fluxes clearly decreased by factors of $1.6-2.6$ between the two intervals, one cannot conclude that the spectral shape changed for any of the sources considering the measurement uncertainties. For V407 Cyg, these conclusions are again consistent with (3).

S2. High-energy Proton and Electron Spectra

Hadronic Model

Following (3), the γ-ray spectra due to the decay of π^0 produced in pp collisions was calculated following the method presented in (34), assuming a Solar metallicity (35). We use high-energy proton spectra in the form $N_p(p_p) = N_{p,0}(p_p c)^{-s_p}e^{-W_p/E_{cp}}$ (proton/GeV), where p_p is the proton momentum and W_p is the kinetic energy of protons [see, e.g., (36)]. The parameters that were fitted to the data are $N_{p,0}$, s_p and E_{cp} which are the normalization, the slope, and the cutoff energy of the high-energy proton spectrum, respectively. The fits were performed using the `gtlike` likelihood fitting tool. The corresponding best-fit parameters and TS values obtained for each nova are presented in Table S1. The best-fit models are shown in Fig. 3 and the

5

corresponding confidence regions of the slopes and cutoff energy fits are presented in Fig. S3. These contour plots have similar shapes except the one for V407 Cyg, which shows a deep χ^2 minimum at a slope of 1.4; one can also see a secondary χ^2 minimum at about the value we published in (3).

The total energy in high-energy protons can be calculated using estimates of the mean local target density over the time interval when the γ rays were detected. In the hadronic model, we assumed that high-energy protons collide with the nuclei of the ejecta, except for V407 Cyg where the ejecta expand in the dense stellar wind of the companion star (3). Consequently, in the latter case, high-energy protons collide with hydrogen nuclei that are in the ejecta and the wind. The high-energy protons are assumed to be uniformly distributed in the ejecta, which is transparent to >100 MeV γ rays. For the three classical novae, the mean density of target hydrogen is assumed to correspond to the ejecta mass in the mean ejecta volume. Despite the likelihood that the ejecta are axisymmetric rather than spherical, for simplicity we calculated the mean ejecta volume over the γ-ray emission duration assuming an expanding shell with an outer radius $R_{\text{out}}(t) = v_{\text{ej}} \times t$ and a relative thickness $\Delta R/R_{\text{out}} \approx 0.4$ [see, e.g., (9, 20)]. In these conditions, the total energy in high-energy protons (ϵ_{p}) resulting from the best fitting parameters ($N_{\text{p,0}}$, s_{p}, and E_{cp}) is about $10^{42} - 10^{43}$ ergs (see Table S3) with proton lifetimes ranging from ~ 100 to 300 days. The corresponding ratios η_{p} of the total energy in high-energy protons to the kinetic energy of the ejecta are presented with the ejecta parameters in Table S3. The conversion efficiencies η_{p} in Table S3 are similar to those estimated in supernova remnants [e.g., (37) and references therein]. The γ-ray emission produced by the secondary electrons and positrons from high-energy proton interactions with ejecta nuclei was not taken into account in this study since it requires more detailed modeling of the novae. This γ-ray emission component would contribute to the low energy range of the LAT spectra since the secondary lepton spectrum has a bump shape that peaks at $\sim$100 MeV. As the γ-ray emissivity is proportional to the number of target nuclei, the values of ϵ_{p} and η_{p} presented in Table S3 scale with the ejecta mass as M_{ej}^{-1} and M_{ej}^{-2}, respectively.

Leptonic Model

In the leptonic model, the inverse Compton (IC) and bremsstrahlung spectra are calculated using the method presented in (38), for a high-energy electron spectrum that is an exponentially cutoff power-law: $N_{\text{e}}(W_{\text{e}}) = N_{\text{e,0}}W_{\text{e}}^{-s_{\text{e}}}e^{-W_{\text{e}}/E_{\text{ce}}}$ (electron/GeV), where W_{e} is the kinetic energy of electrons. As in the hadronic model, the normalization ($N_{\text{e,0}}$), the slope (s_{e}) and the cutoff energy (E_{ce}) were fitted to the LAT data with the `gtlike` likelihood fitting tool. The results of the fit for each nova are presented in Table S1 and the corresponding confidence regions of the slope and cutoff energy fit in Fig. S4. The best-fit models are presented in Fig. 3.

The target photons used to calculate the γ-ray spectrum produced by the IC process are emitted by the nova photosphere. This differs from the first study of the V407 Cyg γ-ray emission (3) for which the target photons were assumed to be emitted by the red giant (RG)

companion star. The target photon spectrum was modeled by a black body with a temperature of 15 000 K and a radius of 3×10^{12} cm, taken as typical values characterizing nova photospheres. The photon distribution before scattering is assumed to be isotropic in the high energy electron frame. The high-energy electrons were assumed to be at the ejecta front layer, at a distance from the white dwarf that corresponds to the average radius of the ejecta during the γ-ray emission duration, taking into account the ejecta velocity (v_{ej}) presented in Table S3. In order to estimate the effects of high-energy electron interactions with the atoms in the ejecta, we calculated the bremsstrahlung spectrum assuming that high-energy electrons interact with a canonical ejecta mass of $10^{-5}M_{\odot}$ (Solar metallicity), except for V407 Cyg where the additional target atoms in the dense stellar wind of the companion red giant star were taken into account (*3*). The separate contributions of the IC and bremsstrahlung spectral components in the best-fit leptonic models are presented in Fig. S5. The model parameters fitted with the LAT data led to the total high-energy electron energies and conversion efficiencies presented in Table S4. The resulting electron lifetimes range from ∼4 to 10 days. The conversion efficiencies were calculated assuming kinetic energies derived from ejecta parameters presented in Table S3. It should be noted that the values of the total energy of high-energy electrons obtained from the fits scale with the inverse of the nova luminosity since more target photons implies fewer high-energy electrons are needed to produce the same γ-ray luminosity.

S3. Notes on Available Optical Observations of the Novae

V407 Cyg 2010

The symbiotic binary system V407 Cyg was studied in detail by (*19*), who found that the secondary is a Mira variable with spectral type M6 III and distance of 2.7 kpc as assumed here and in our previous LAT γ-ray detection paper on the 2010 nova (*3*).

V959 Mon 2012

The historical optical and near-infrared counterpart of Nova Monocerotis 2012 (V959 Mon) was found in archival databases by (*39*). These consisted of optical observations ($r \simeq 17.8 - 18.1$ and $i = 17.1 - 17.4$ mag) from the INT Photometric H-Alpha Survey that used the 2.5m Isaac Newton Telescope and near-infrared photometry ($J = 16.26$, $H = 15.71$, and $K = 15.42$ mag) from the UKIDSS survey that used the 3.8m UK Infrared Telescope. Considering a plausible range of values of the extinction $E(B - V) = 0.3 - 0.8$ [see also (*9*)], (*39*) concluded that the companion is likely a main-sequence star.

V1324 Sco 2012

The available multi-wavelength observations of Nova Scorpii 2012 (V1324 Sco) are relatively sparse compared to V959 Mon and V339 Del. In the report of its optical discovery, (*15*) found

a variable pre-outburst counterpart with $I = 19.0 - 19.5$ mag. The AAVSO light curve shows a V-band maximum around 10th mag. The B magnitude at maximum was about 11.5 which, assuming an intrinsic $(B - V)_0 \sim 0$ [e.g., (*40*)], implies a large $E(B - V)$ value of 1.5 mag. With a time of decline by two magnitudes t_2 of about 25 days estimated from the AAVSO light curve, we obtain an absolute V-band magnitude of -7.6 from the maximum magnitude rate of decline relation of (*41*) and a distance of 4 kpc. We emphasize the uncertainty in this method (*29*) and adopted it in the absence of any more direct method for obtaining the intrinsic properties. Note, however, that the substantial drop in brightness might be from a dust-forming event that compromises the t_2 value; without dust formation the t_2 time would be much longer and the inferred source closer. The same applies if the extinction has been overestimated. For example if $E(B - V) \sim 1$ mag, which might be supported by the low neutral hydrogen column density toward this source, the distance is 8 kpc. Given the uncertainties outlined, we adopted the distance of 4.5 kpc from (*17*) and the absolute magnitude of the quiescent counterpart in the I-band is ~ 2 mag.

V339 Del 2013

Nova Delphini 2013 (V339 Del) was discovered as PNV J20233073+2046041 by Koichi Itagaki (Teppo-cho, Yamagata, Japan) at 6.8 magnitude on 2013 August 14.584 UT with nothing visible in an image taken with a limiting magnitude of 13.0 on August 13.565 (*11*). Optical spectroscopy identified it as a classical nova (*14,42,43*). Pre-discovery images indicated a rapid brightening from 10.1 to 8.5 magnitude from 7hr UT to 8hr UT on the discovery date (*44*). The historical $V = 17.1$ mag of the optical counterpart comes from APASS observations (*45*); see also (*46*). With the small extinction $E(B - V) \simeq 0.2$ (*43,47,48*), the absolute magnitude is 3.5 mag making this unlikely a red giant. We obtained V-band magnitudes from the American Association of Variable Star Observers (AAVSO)[6] (*49*), averaged them in 0.25 day bins, and these are plotted along with the γ-ray light curves (Fig. S6). The naked-eye peak visual 4.3 magnitude, also from the AAVSO, was observed on 2013 August 16.5, two days after discovery.

---

[6]http://www.aavso.org/lcg
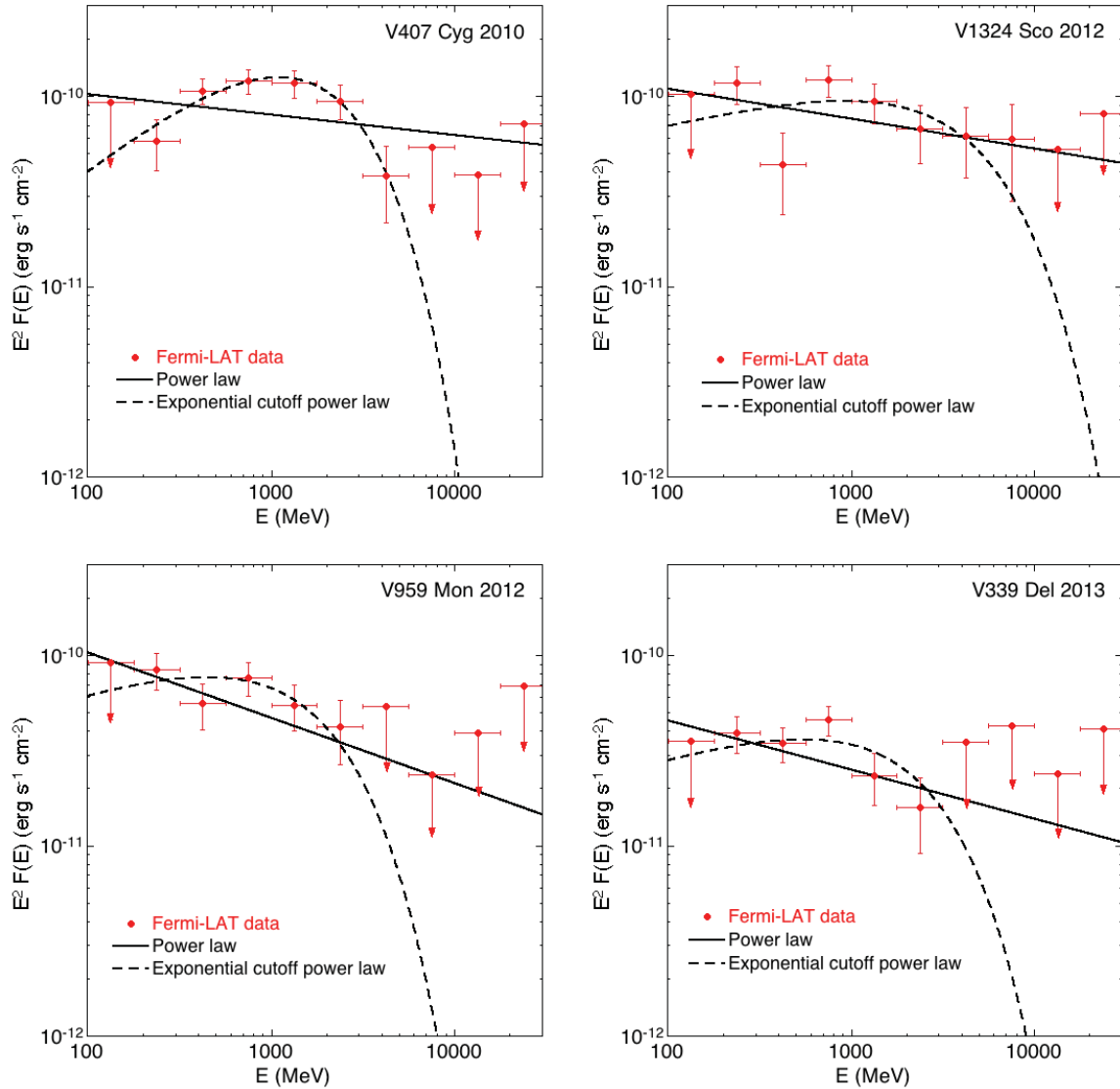
Fig. S1. Fermi-LAT >100 MeV average γ-ray spectra of the four novae over the full $17-27$ day durations. Vertical bars indicate 1σ uncertainties for data points with $TS > 4$; otherwise, arrows indicate 2σ limits. The best-fit PL and EPL models (Table S1) are overlaid on the LAT data.
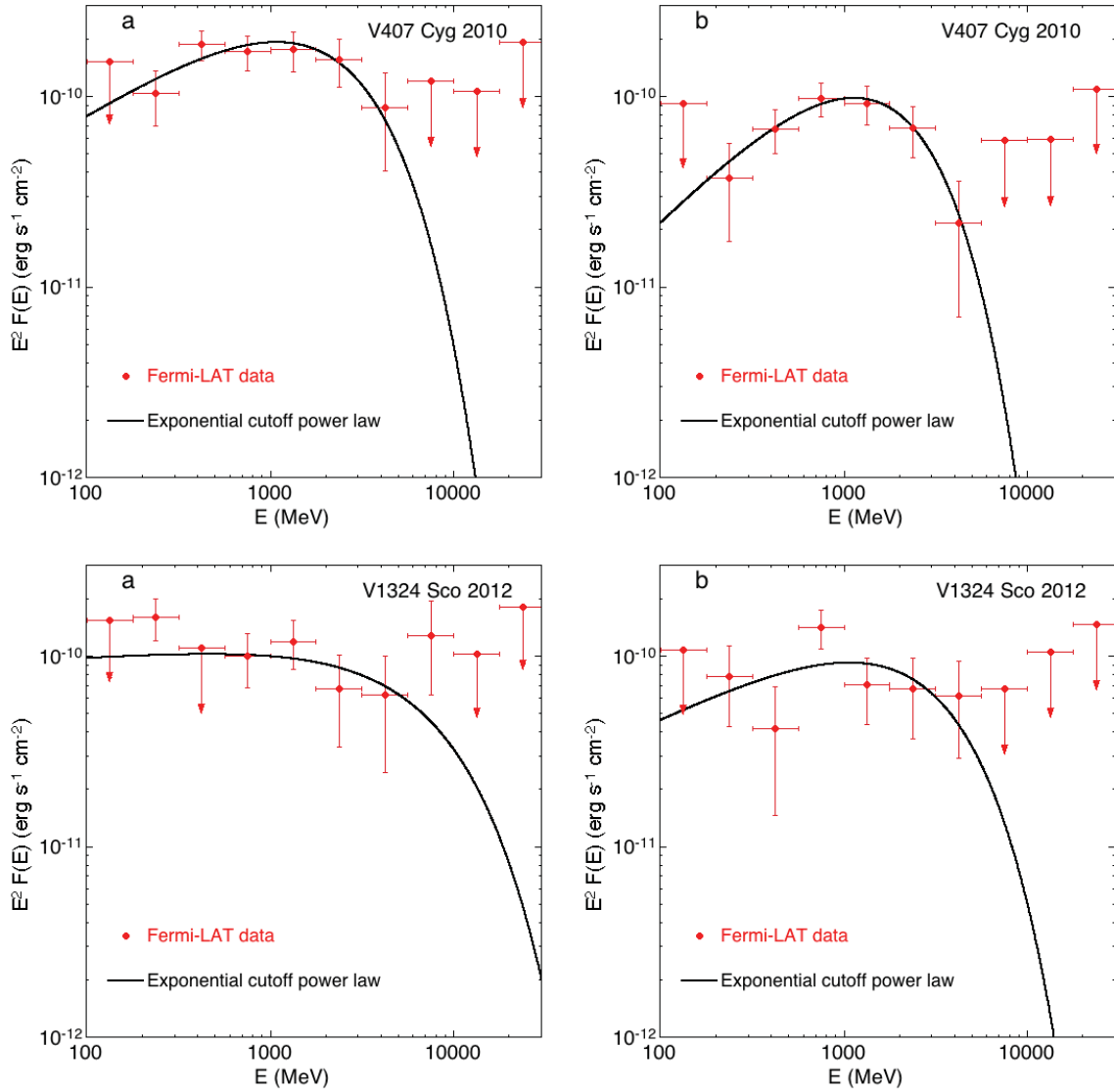
Fig. S2. Fermi-LAT >100 MeV average γ-ray spectra of the four novae as in Fig. S1 but split into two intervals denoted as panels (a) and (b). Vertical bars indicate 1σ uncertainties for data points with $TS > 4$; otherwise, arrows indicate 2σ limits. The best-fit EPL models are overlaid onto the LAT data. See Table S1 for details.
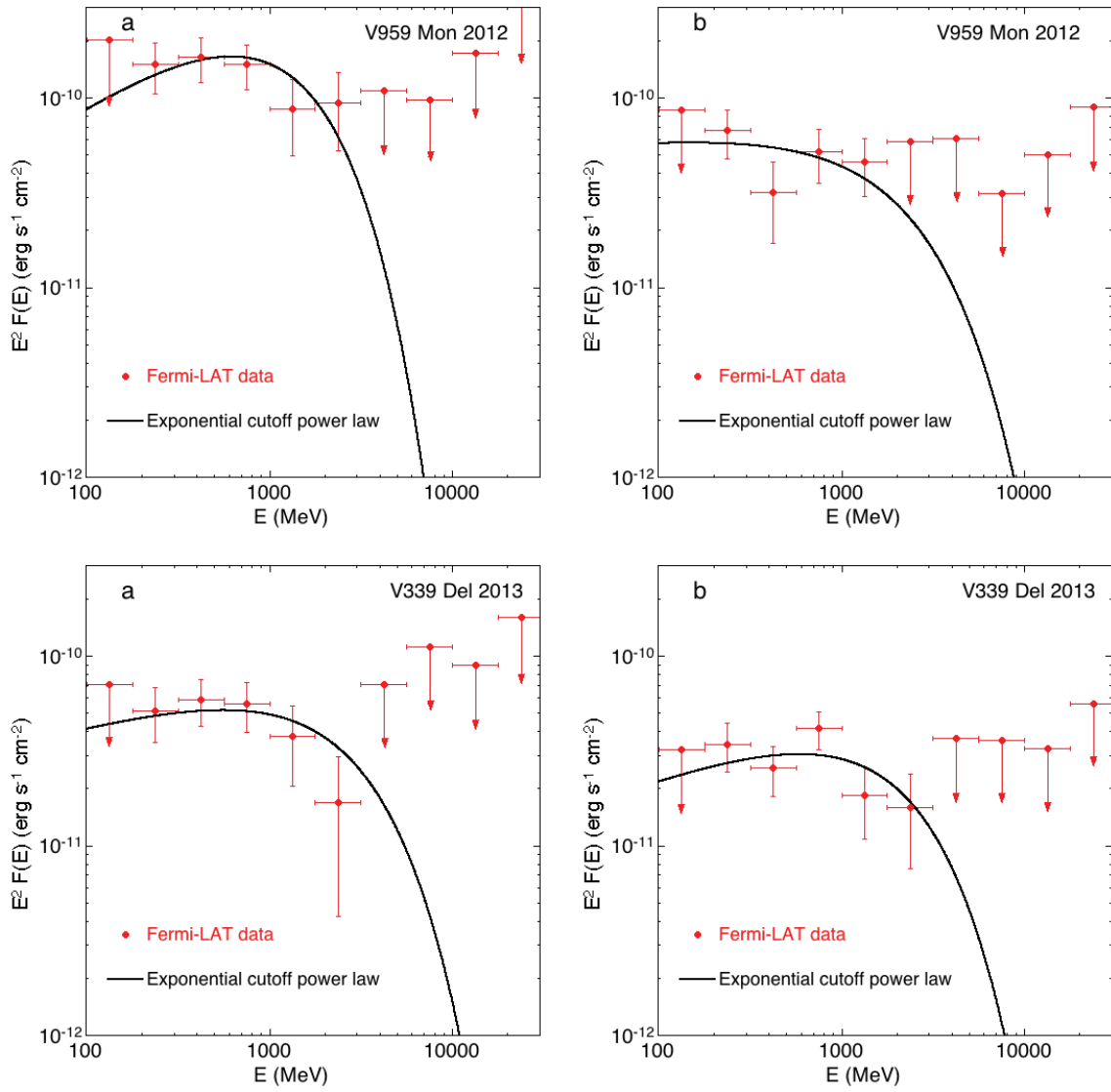
Fig. S2. *continued.*
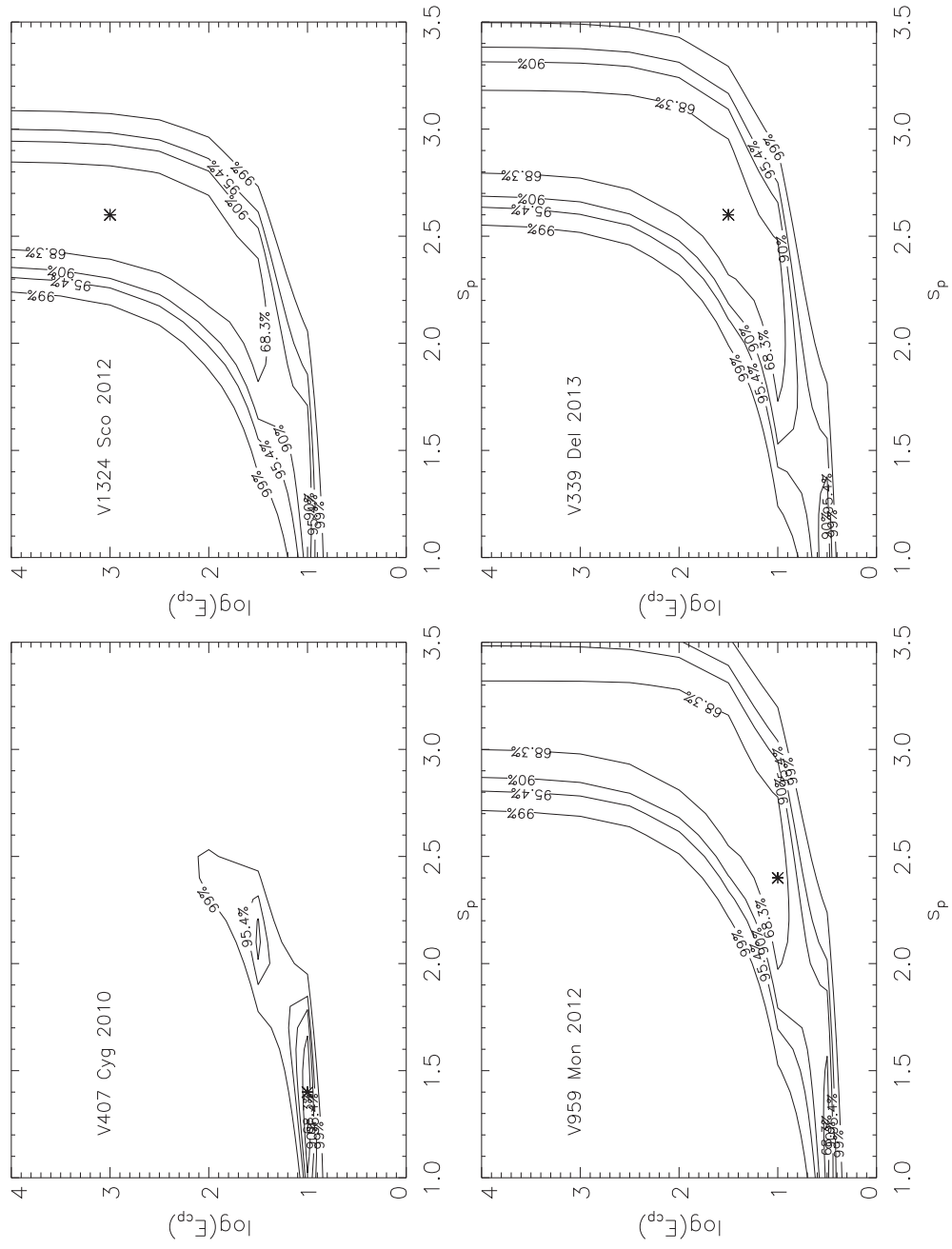
Fig. S3. Contour plots of the hadronic model fits of the high-energy proton spectral parameters for the four novae (energies *E* in units of GeV). The star symbol in each panel indicates the best-fit value (see Table **S1**).
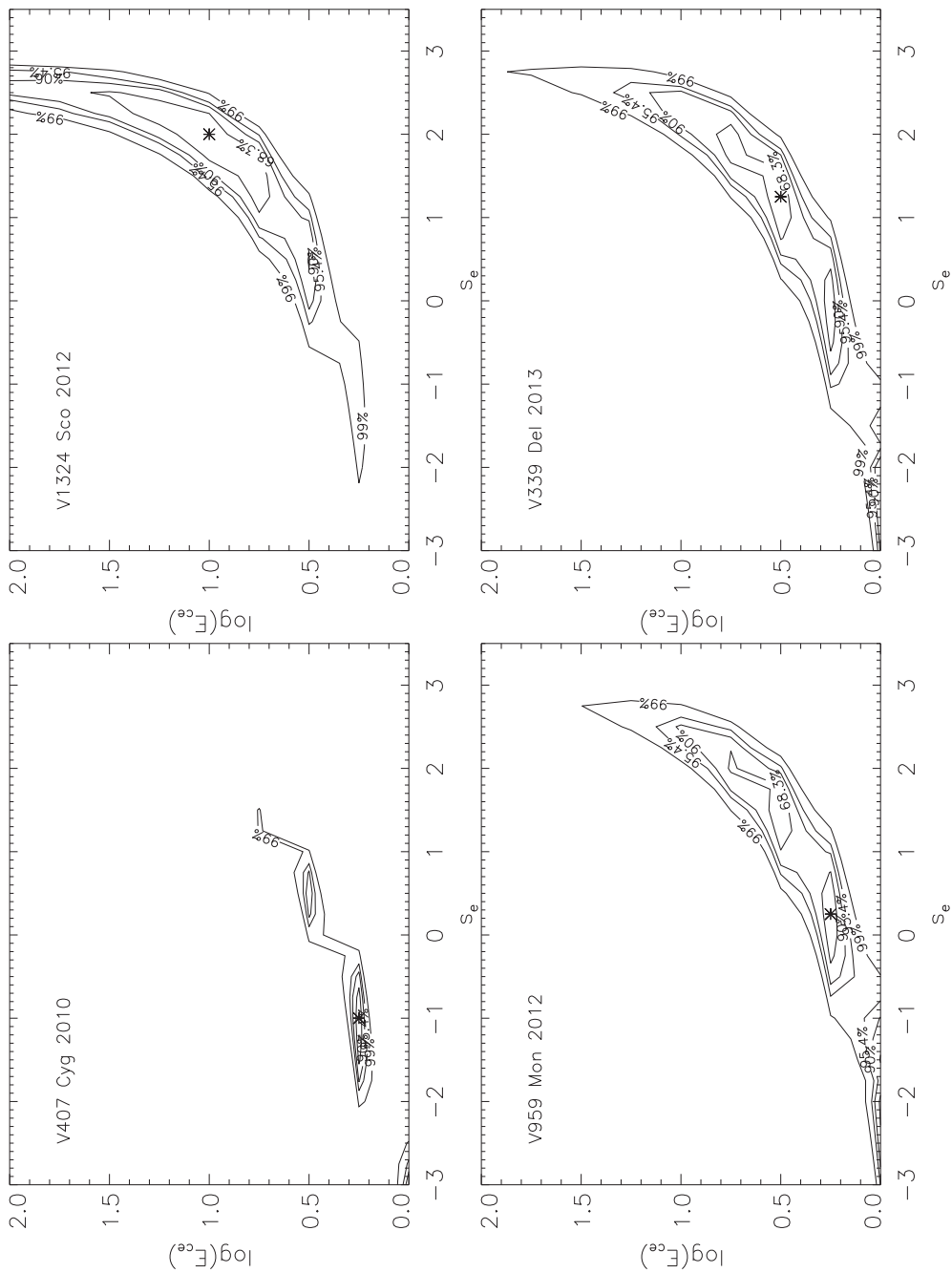
Fig. S4. As in Fig. S3, but for the leptonic model fits of the high-energy electron spectral parameters.
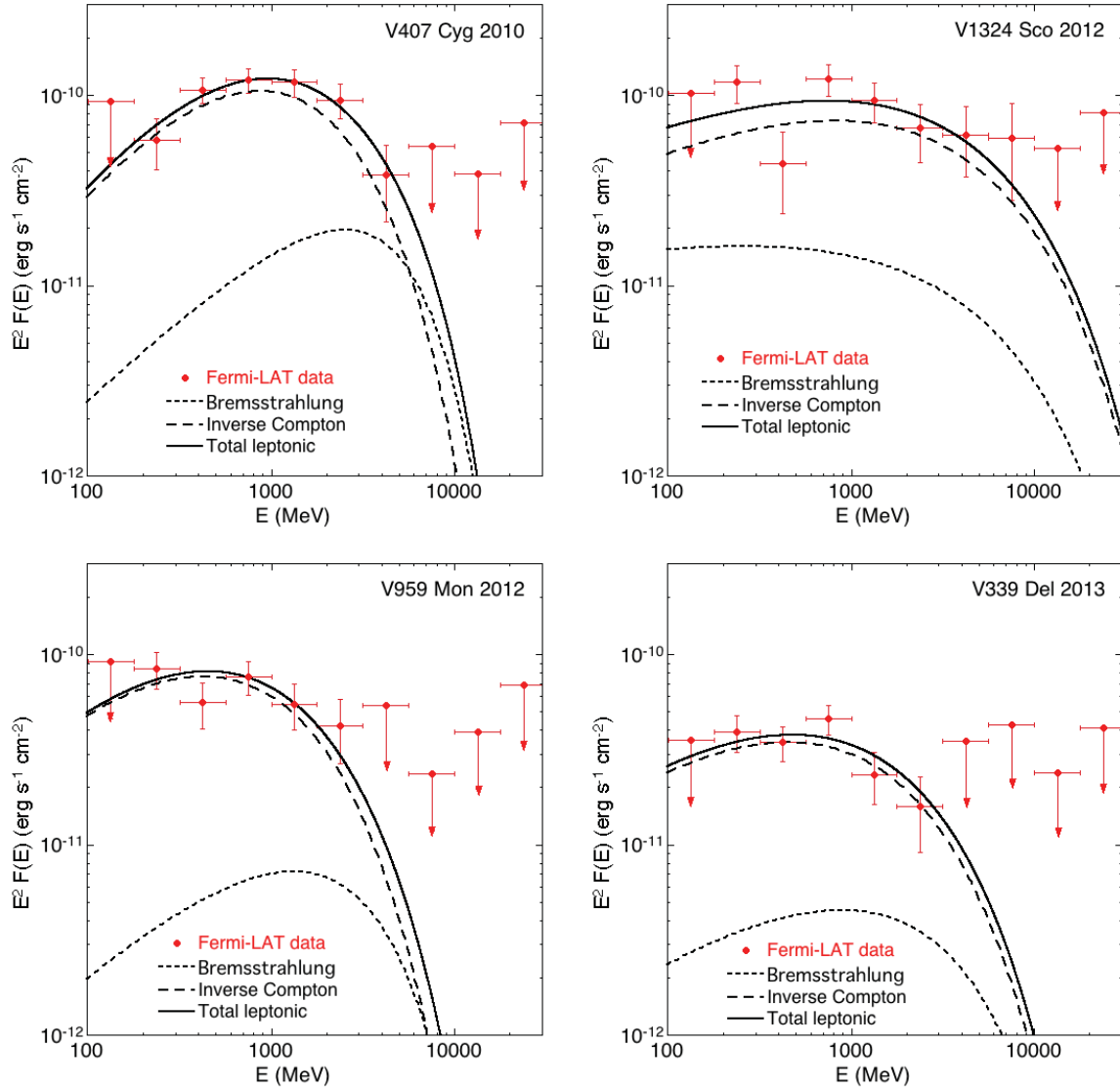
Fig. S5. Fermi-LAT >100 MeV average γ-ray spectra of the four novae over the full 17−27 day durations (as shown in Fig. 3) showing the inverse Compton and bremsstrahlung spectral components in the leptonic model as well as their total.

14
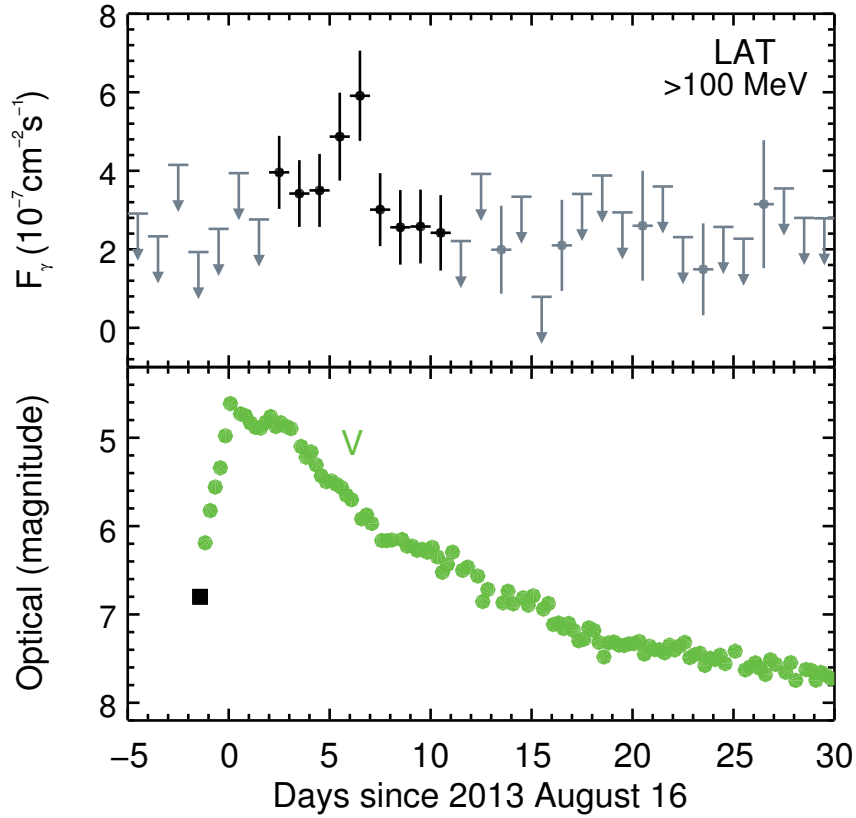
Fig. S6. Fermi-LAT 1-day binned light curve (top panel) of V339 Del as shown in Fig. 2 where vertical bars indicate 1σ uncertainties for data points with $TS > 9$ (black) and $TS = 4-9$ (gray), while gray arrows indicate 2σ limits when $TS < 4$. The γ-ray light curve is compared to the 0.25 day binned optical V-band AAVSO light curve (green circles) for the same time interval (bottom panel) with the inclusion of the unfiltered discovery magnitude (black square) from (*11*).

Nova	V407 Cyg 2010	V1324 Sco 2012	V959 Mon 2012	V339 Del 2013
Single Power Law				
Flux	5.77 ± 0.55	5.90 ± 0.87	4.81 ± 0.59	2.26 ± 0.28
Photon index	2.11 ± 0.06	2.16 ± 0.09	2.34 ± 0.09	2.26 ± 0.08
TS	366.5	178.5	156.0	197.5
Exponentially Cutoff Power Law				
Flux	4.30 ± 0.54	4.93 ± 2.45	4.13 ± 0.60	1.93 ± 0.29
Slope, s	1.23 ± 0.20	1.77 ± 0.68	1.69 ± 0.25	1.72 ± 0.24
E_c	1.44 ± 0.36	4.10 ± 6.14	1.45 ± 0.61	1.94 ± 0.95
TS	408.1	184.6	170.3	208.9
Exponentially Cutoff Power Law split into intervals: (a), (b)				
MJD start	55265, 55271	56093, 56099	56097, 56103	56520, 56526
Interval (days)	6, 16	6, 11	6, 16	6, 21
Flux	7.39 ± 1.07, 2.84 ± 0.61	6.11 ± 1.37, 3.92 ± 1.10	7.33 ± 1.47, 3.32 ± 0.66	2.81 ± 0.54, 1.56 ± 0.34
Slope, s	1.39 ± 0.22, 1.00 ± 0.38	1.94 ± 0.23, 1.53 ± 0.35	1.35 ± 0.38, 1.92 ± 0.31	1.75 ± 0.31, 1.65 ± 0.35
E_c	1.78 ± 0.63, 1.14 ± 0.43	7.08 ± 6.00, 2.25 ± 1.33	0.95 ± 0.43, 1.97 ± 1.42	2.21 ± 1.69, 1.67 ± 1.03
TS	261.7, 176.6	110.9, 76.7	117.3, 73.9	108.3, 108.3
Hadronic Modeling				
Flux	$4.05^{+0.26}_{-0.37}$	$4.25^{+0.54}_{-0.77}$	$3.66^{+0.44}_{-0.46}$	$1.75^{+0.23}_{-0.20}$
E_{cp}	$10^{+1.0}_{-0.7}$	> 32	> 3.2	> 10
Slope, s_p	$1.4^{+0.3}_{-0.4}$	$2.6^{+0.2}_{-0.7}$	$2.4^{+0.9}_{-1.4}$	$2.6^{+0.5}_{-0.8}$
TS	402.7	180.7	168.4	211.2
Leptonic Modeling				
Flux	$4.12^{+0.27}_{-0.50}$	$4.91^{+0.64}_{-0.87}$	$3.96^{+0.62}_{-0.55}$	$1.93^{+0.16}_{-0.34}$
E_{ce}	1.78 ± 0.05	10^{+22}_{-7}	$1.8^{+3.8}_{-0.8}$	$3.2^{+2.5}_{-1.4}$
Slope, s_e	$-1.0^{+0.25}_{-0.5}$	$2.0^{+0.5}_{-1.5}$	$0.25^{+1.75}_{-0.55}$	$1.25^{+0.75}_{-1.75}$
TS	403.1	181.8	169.7	210.0

Table S1. LAT γ-ray spectral fit results, model parameters, and best-fit results from the hadronic and leptonic modeling. Fluxes at >100 MeV energies are in units of 10^{-7} photons cm^{-2} s^{-1} and the cutoff energies E_c in GeV. The reported errors on spectral parameters are 1σ uncertainties and statistical only. We estimate that the systematic uncertainties are comparable or smaller, $\sim 8\%$ for the fluxes and ~ 0.1 in photon indices (32).

Days since	V407 Cyg 2010		V1324 Sco 2012		V959 Mon 2012		V339 Del 2013	
start	TS	F_γ	TS	F_γ	TS	F_γ	TS	F_γ
-4.5	3.0	< 7.2	0.0	< 4.2	0.3	< 6.0	0.0	< 2.9
-3.5	0.0	< 3.0	0.5	< 4.2	0.0	< 4.8	0.0	< 2.3
-2.5	0.0	< 2.2	0.2	< 3.6	0.5	< 6.7	1.7	< 4.2
-1.5	3.5	< 6.6	2.7	< 6.1	0.2	< 5.8	0.0	< 1.9
-0.5	0.0	< 3.4	3.0	< 7.1	1.7	< 9.1	0.0	< 2.5
0.5	16.2	6.2 ± 2.2	9.0	3.7 ± 1.9	9.0	5.4 ± 2.5	3.3	< 3.9
1.5	58.9	11.1 ± 2.3	14.1	6.9 ± 2.3	9.6	7.6 ± 3.2	1.1	< 2.8
2.5	12.8	5.9 ± 2.1	14.9	6.7 ± 2.4	14.4	8.4 ± 2.9	42.6	4.0 ± 0.9
3.5	68.6	13.1 ± 2.5	16.0	7.1 ± 2.4	32.8	12.9 ± 3.5	37.2	3.4 ± 0.8
4.5	56.8	13.9 ± 2.6	23.0	8.8 ± 2.7	27.9	10.6 ± 3.1	25.3	3.5 ± 0.9
5.5	47.9	13.2 ± 2.7	33.4	10.9 ± 2.7	27.7	13.8 ± 3.7	38.8	4.9 ± 1.1
6.5	27.1	7.5 ± 2.1	35.0	12.3 ± 2.9	15.7	9.8 ± 3.2	65.7	5.9 ± 1.1
7.5	10.1	5.6 ± 2.3	14.3	7.6 ± 2.6	11.3	8.0 ± 3.1	25.8	3.0 ± 0.9
8.5	11.0	4.7 ± 1.9	2.1	< 7.9	29.2	13.5 ± 3.6	14.4	2.6 ± 0.9
9.5	35.1	10.3 ± 2.5	15.5	10.3 ± 3.3	3.3	< 8.3	17.5	2.6 ± 0.9
10.5	12.5	3.9 ± 1.8	2.6	< 9.0	1.7	< 7.2	10.8	2.4 ± 1.0
11.5	20.6	6.5 ± 2.3	10.3	6.7 ± 3.0	15.1	9.1 ± 3.1	0.9	< 2.2
12.5	1.1	< 5.3	0.0	< 5.8	2.8	< 8.5	2.5	< 3.9
13.5	11.7	6.8 ± 2.6	0.0	< 5.4	4.8	4.8 ± 2.7	5.0	2.0 ± 1.1
14.5	16.5	6.5 ± 2.3	7.0	9.5 ± 4.3	2.3	< 7.0	1.3	< 3.3
15.5	14.8	7.2 ± 2.5	1.7	< 7.2	0.0	< 3.6	0.0	< 0.8
16.5	1.1	< 6.2	6.4	8.7 ± 4.3	1.9	< 3.6	6.0	2.1 ± 1.2
17.5	8.0	4.5 ± 2.1	0.7	< 10.6	0.0	< 1.6	1.0	< 3.4
18.5	0.0	< 3.0	0.0	< 6.5	0.0	< 2.4	1.9	< 3.9
19.5	4.4	3.0 ± 2.0	0.9	< 9.6	6.3	2.6 ± 1.3	1.4	< 2.9
20.5	1.4	< 7.5	0.0	< 31.1	4.3	3.8 ± 2.2	7.9	2.6 ± 1.4
21.5	4.1	3.8 ± 2.3	0.1	< 7.6	7.9	3.9 ± 2.0	0.4	< 3.6
22.5	2.3	< 9.3	0.0	< 5.6	0.0	< 4.8	0.0	< 2.3
23.5	0.1	< 5.4	2.5	< 12.8	0.3	< 5.6	4.1	1.5 ± 1.2
24.5	0.0	< 3.7	0.0	< 4.1	0.0	< 2.0	0.1	< 2.6
25.5	3.0	< 8.7	0.4	< 9.8	0.0	< 4.5	0.0	< 2.3
26.5	0.5	< 5.2	0.4	< 9.4	2.5	< 6.7	6.1	3.1 ± 1.6
27.5	3.4	< 3.0	0.0	< 6.7	0.0	< 3.5	0.1	< 3.5
28.5	0.0	< 1.5	0.0	< 6.2	0.6	< 5.7	0.0	< 2.8
29.5	0.3	< 3.0	0.3	< 9.4	2.9	< 7.6	0.0	< 2.8

Table S2. Daily LAT γ-ray TS and >100 MeV fluxes F_γ in units of 10^{-7} photons cm^{-2} s^{-1} and 95% confidence upper limits (when $TS < 4$) corresponding to Fig. 2 in the main paper. The dates indicated are the centers of the one day bins relative to the defined start times (t_{s}).

Nova	V407 Cyg 2010	V1324 Sco 2012	V959 Mon 2012	V339 Del 2013
$\dot{\epsilon}_\gamma^{\pi^0}$ (10^{35} erg s^{-1})	$3.04^{+0.04}_{-0.03}$	$9.12^{+0.54}_{-0.93}$	$3.50^{+0.27}_{-0.14}$	$2.52^{+0.23}_{-0.11}$
$M_{\rm ej}$ ($M_\odot$)	10^{-6}	10^{-5}	6×10^{-5}	8×10^{-5}
$v_{\rm ej}$ (km s^{-1})	3200	2200	3000	2000
$\epsilon_{\rm p}$ (10^{42} erg)	$6.8^{+0.4}_{-0.5}$	$17.2^{+7.8}_{-1.5}$	$10.1^{+5.4}_{-2.6}$	$3.0^{+0.9}_{-0.7}$
$\eta_{\rm p}$ (%)	$6.6^{+0.4}_{-0.5}$	$3.7^{+0.2}_{-0.4}$	$0.19^{+0.10}_{-0.05}$	$0.09^{+0.03}_{-0.02}$
$F_\epsilon^{\pi^0}$ (10^{-10} erg s^{-1} cm^{-2})	$3.46^{+0.04}_{-0.03}$	$3.73^{+0.22}_{-0.38}$	$2.23^{+0.17}_{-0.09}$	$1.18^{+0.11}_{-0.05}$

Table S3. Best-fit γ-ray luminosity for the hadronic models ($\dot{\epsilon}_\gamma^{\pi^0}$) and ejecta parameters used to calculate the energetics of the novae. $M_{\rm ej}$ is the mass of the ejecta, $v_{\rm ej}$ is the ejecta velocity, $\epsilon_{\rm p}$ is the total energy in protons, $\eta_{\rm p}$ is the conversion efficiency, and $F_\epsilon^{\pi^0}$ is the total energy flux. The 1σ uncertainties were obtained from the fits of the models to the LAT data.

Nova	V407 Cyg 2010	V1324 Sco 2012	V959 Mon 2012	V339 Del 2013
$\dot{\epsilon}_\gamma^{\rm IC}$ (10^{35} erg s^{-1})	$3.11^{+0.04}_{-0.06}$	$9.42^{+1.04}_{-1.18}$	$3.80^{+0.36}_{-0.29}$	$2.67^{+0.15}_{-0.20}$
$\epsilon_{\rm e}$ (10^{41} erg)	5.9 ± 0.1	$13.4^{+3.1}_{-2.1}$	$8.0^{+4.4}_{-1.1}$	$6.6^{+1.3}_{-0.7}$
$\eta_{\rm e}$ (%)	0.57 ± 0.01	$0.28^{+0.06}_{-0.04}$	$0.09^{+0.05}_{-0.01}$	$0.17^{+0.03}_{-0.02}$
$F_\epsilon^{\rm IC}$ (10^{-10} erg s^{-1} cm^{-2})	$3.53^{+0.05}_{-0.07}$	$3.85^{+0.43}_{-0.48}$	$2.43^{+0.23}_{-0.19}$	$1.25^{+0.07}_{-0.09}$

Table S4. Best-fit γ-ray luminosity for the leptonic models ($\dot{\epsilon}_\gamma^{\rm IC}$), total energy in electrons ($\epsilon_{\rm e}$), conversion efficiency ($\eta_{\rm e}$), and $F_\epsilon^{\rm IC}$ the total energy flux obtained for the four novae. The 1σ uncertainties were obtained from the fits of the models to the LAT data.

The Fermi-LAT Collaboration: M. Ackermann[1], M. Ajello[2], A. Albert[3], L. Baldini[4], J. Ballet[5], G. Barbiellini[6,7], D. Bastieri[8,9], R. Bellazzini[4], E. Bissaldi[10], R. D. Blandford[3], E. D. Bloom[3], E. Bottacini[3], T. J. Brandt[11], J. Bregeon[12], P. Bruel[13], R. Buehler[1], S. Buson[8,9], G. A. Caliandro[3,14], R. A. Cameron[3], M. Caragiulo[15], P. A. Caraveo[16], E. Cavazzuti[17], E. Charles[3], A. Chekhtman[18], C. C. Cheung[19]†, J. Chiang[3], G. Chiaro[9], S. Ciprini[17,20], R. Claus[3], J. Cohen-Tanugi[12], J. Conrad[21,22,23,24], S. Corbel[5,25], F. D'Ammando[26,27], A. de Angelis[28], P. R. den Hartog[3], F. de Palma[15], C. D. Dermer[19], R. Desiante[6,29], S. W. Digel[3], L. Di Venere[30], E. do Couto e Silva[3], D. Donato[31,32], P. S. Drell[3], A. Drlica-Wagner[33], C. Favuzzi[30,15], E. C. Ferrara[11], W. B. Focke[3], A. Franckowiak[3], L. Fuhrmann[34], Y. Fukazawa[35], P. Fusco[30,15], F. Gargano[15], D. Gasparrini[17,20], S. Germani[36,37], N. Giglietto[30,15], F. Giordano[30,15], M. Giroletti[26], T. Glanzman[3], G. Godfrey[3], I. A. Grenier[5], J. E. Grove[19], S. Guiriec[11,38], D. Hadasch[39], A. K. Harding[11], M. Hayashida[40], E. Hays[11], J.W. Hewitt[41,31], A. B. Hill[42,3,43], X. Hou[44], P. Jean[45,46]†, T. Jogler[3], G. Jóhannesson[47], A. S. Johnson[3], W. N. Johnson[19], M. Kerr[48], J. Knödlseder[45,46], M. Kuss[4], S. Larsson[21,22,49], L. Latronico[50], M. Lemoine-Goumard[44,51], F. Longo[6,7], F. Loparco[30,15], B. Lott[44], M. N. Lovellette[19], P. Lubrano[36,37], A. Manfreda[4], P. Martin[46], F. Massaro[52], M. Mayer[1], M. N. Mazziotta[15], J. E. McEnery[11,32], P. F. Michelson[3], W. Mitthumsiri[53,3], T. Mizuno[54], M. E. Monzani[3], A. Morselli[55], I. V. Moskalenko[3], S. Murgia[56], R. Nemmen[11,31,41], E. Nuss[12], T. Ohsugi[54], N. Omodei[3], M. Orienti[26], E. Orlando[3], J. F. Ormes[57], D. Paneque[58,3], J. H. Panetta[3], J. S. Perkins[11], M. Pesce-Rollins[4], F. Piron[12], G. Pivato[9], T. A. Porter[3], S. Rainò[30,15], R. Rando[8,9], M. Razzano[4,59], S. Razzaque[60], A. Reimer[39,3], O. Reimer[39,3], T. Reposeur[44], P. M. Saz Parkinson[61,62], M. Schaal[63], A. Schulz[1], C. Sgrò[4], E. J. Siskind[64], G. Spandre[4], P. Spinelli[30,15], Ł. Stawarz[65,66], D. J. Suson[67], H. Takahashi[35], T. Tanaka[68], J. G. Thayer[3], J. B. Thayer[3], D. J. Thompson[11], L. Tibaldo[3], M. Tinivella[4], D. F. Torres[69,70], G. Tosti[36,37], E. Troja[11,32], Y. Uchiyama[71], G. Vianello[3], B. L. Winer[72], M. T. Wolff[19], D. L. Wood[73], K. S. Wood[19], M. Wood[3], S. Charbonnel[74], R. H. D. Corbet[31,41], I. De Gennaro Aquino[75,76], J. P. Edlin[77], E. Mason[78], G. J. Schwarz[79], S. N. Shore[4,75]†, S. Starrfield[80], F. Teyssier[81]

1. Deutsches Elektronen Synchrotron DESY, D-15738 Zeuthen, Germany

2. Department of Physics and Astronomy, Clemson University, Kinard Lab of Physics, Clemson, SC 29634-0978, USA

3. W. W. Hansen Experimental Physics Laboratory, Kavli Institute for Particle Astrophysics and Cosmology, Department of Physics and SLAC National Accelerator Laboratory, Stanford University, Stanford, CA 94305, USA

4. Istituto Nazionale di Fisica Nucleare, Sezione di Pisa, I-56127 Pisa, Italy

5. Laboratoire AIM, CEA-IRFU/CNRS/Université Paris Diderot, Service d'Astrophysique, CEA Saclay, 91191 Gif sur Yvette, France

6. Istituto Nazionale di Fisica Nucleare, Sezione di Trieste, I-34127 Trieste, Italy

7. Dipartimento di Fisica, Università di Trieste, I-34127 Trieste, Italy

8. Istituto Nazionale di Fisica Nucleare, Sezione di Padova, I-35131 Padova, Italy

9. Dipartimento di Fisica e Astronomia "G. Galilei", Università di Padova, I-35131 Padova, Italy

10. Istituto Nazionale di Fisica Nucleare, Sezione di Trieste, and Università di Trieste, I-34127 Trieste, Italy

11. NASA Goddard Space Flight Center, Greenbelt, MD 20771, USA

12. Laboratoire Univers et Particules de Montpellier, Université Montpellier 2, CNRS/IN2P3, Montpellier, France

13. Laboratoire Leprince-Ringuet, École polytechnique, CNRS/IN2P3, Palaiseau, France

14. Consorzio Interuniversitario per la Fisica Spaziale (CIFS), I-10133 Torino, Italy

15. Istituto Nazionale di Fisica Nucleare, Sezione di Bari, 70126 Bari, Italy

16. INAF-Istituto di Astrofisica Spaziale e Fisica Cosmica, I-20133 Milano, Italy

17. Agenzia Spaziale Italiana (ASI) Science Data Center, I-00133 Roma, Italy

18. Center for Earth Observing and Space Research, College of Science, George Mason University, Fairfax, VA 22030, resident at Naval Research Laboratory, Washington, DC 20375, USA

19. Space Science Division, Naval Research Laboratory, Washington, DC 20375-5352, USA

20. Istituto Nazionale di Astrofisica - Osservatorio Astronomico di Roma, I-00040 Monte Porzio Catone (Roma), Italy

21. Department of Physics, Stockholm University, AlbaNova, SE-106 91 Stockholm, Sweden

22. The Oskar Klein Centre for Cosmoparticle Physics, AlbaNova, SE-106 91 Stockholm, Sweden

23. Royal Swedish Academy of Sciences Research Fellow, funded by a grant from the K. A. Wallenberg Foundation

24. The Royal Swedish Academy of Sciences, Box 50005, SE-104 05 Stockholm, Sweden

25. Institut universitaire de France, 75005 Paris, France

26. INAF Istituto di Radioastronomia, 40129 Bologna, Italy

27. Dipartimento di Astronomia, Università di Bologna, I-40127 Bologna, Italy

28. Dipartimento di Fisica, Università di Udine and Istituto Nazionale di Fisica Nucleare, Sezione di Trieste, Gruppo Collegato di Udine, I-33100 Udine

29. Università di Udine, I-33100 Udine, Italy

30. Dipartimento di Fisica "M. Merlin" dell'Università e del Politecnico di Bari, I-70126 Bari, Italy

31. Center for Research and Exploration in Space Science and Technology (CRESST) and NASA Goddard Space Flight Center, Greenbelt, MD 20771, USA

32. Department of Physics and Department of Astronomy, University of Maryland, College Park, MD 20742, USA

33. Fermilab, Batavia, IL 60510, USA

34. Max-Planck-Institut für Radioastronomie, Auf dem Hügel 69, 53121 Bonn, Germany

35. Department of Physical Sciences, Hiroshima University, Higashi-Hiroshima, Hiroshima 739-8526, Japan

36. Istituto Nazionale di Fisica Nucleare, Sezione di Perugia, I-06123 Perugia, Italy

37. Dipartimento di Fisica, Università degli Studi di Perugia, I-06123 Perugia, Italy

38. NASA Postdoctoral Program Fellow, USA

39. Institut für Astro- und Teilchenphysik and Institut für Theoretische Physik, Leopold-Franzens-Universität Innsbruck, A-6020 Innsbruck, Austria

40. Institute for Cosmic-Ray Research, University of Tokyo, 5-1-5 Kashiwanoha, Kashiwa, Chiba, 277-8582, Japan

41. Department of Physics and Center for Space Sciences and Technology, University of Maryland Baltimore County, Baltimore, MD 21250, USA

42. School of Physics and Astronomy, University of Southampton, Highfield, Southampton, SO17 1BJ, UK

43. Funded by a Marie Curie IOF, FP7/2007-2013 - Grant agreement no. 275861

44. Centre d'Études Nucléaires de Bordeaux Gradignan, IN2P3/CNRS, Université Bordeaux 1, BP120, F-33175 Gradignan Cedex, France

45. CNRS, IRAP, F-31028 Toulouse cedex 4, France

46. GAHEC, Université de Toulouse, UPS-OMP, IRAP, Toulouse, France

47. Science Institute, University of Iceland, IS-107 Reykjavik, Iceland

48. CSIRO Astronomy and Space Science, Australia Telescope National Facility, Epping NSW 1710, Australia

49. Department of Astronomy, Stockholm University, SE-106 91 Stockholm, Sweden

50. Istituto Nazionale di Fisica Nucleare, Sezione di Torino, I-10125 Torino, Italy

51. Funded by contract ERC-StG-259391 from the European Community

52. Department of Astronomy, Department of Physics and Yale Center for Astronomy and Astrophysics, Yale University, New Haven, CT 06520-8120, USA

53. Department of Physics, Faculty of Science, Mahidol University, Bangkok 10400, Thailand

54. Hiroshima Astrophysical Science Center, Hiroshima University, Higashi-Hiroshima, Hiroshima 739-8526, Japan

55. Istituto Nazionale di Fisica Nucleare, Sezione di Roma "Tor Vergata", I-00133 Roma, Italy

56. Center for Cosmology, Physics and Astronomy Department, University of California, Irvine, CA 92697-2575, USA

57. Department of Physics and Astronomy, University of Denver, Denver, CO 80208, USA

58. Max-Planck-Institut für Physik, D-80805 München, Germany

59. Funded by contract FIRB-2012-RBFR12PM1F from the Italian Ministry of Education, University and Research (MIUR)

60. Department of Physics, University of Johannesburg, PO Box 524, Auckland Park 2006, South Africa

61. Santa Cruz Institute for Particle Physics, Department of Physics and Department of Astronomy and Astrophysics, University of California at Santa Cruz, Santa Cruz, CA 95064, USA

62. Department of Physics, The University of Hong Kong, Pokfulam Road, Hong Kong, China

63. National Research Council Research Associate, National Academy of Sciences, Washington, DC 20001, resident at Naval Research Laboratory, Washington, DC 20375, USA

64. NYCB Real-Time Computing Inc., Lattingtown, NY 11560-1025, USA

65. Institute of Space and Astronautical Science, Japan Aerospace Exploration Agency, 3-1-1 Yoshinodai, Chuo-ku, Sagamihara, Kanagawa 252-5210, Japan

66. Astronomical Observatory, Jagiellonian University, 30-244 Kraków, Poland

67. Department of Chemistry and Physics, Purdue University Calumet, Hammond, IN 46323-2094, USA

68. Department of Physics, Graduate School of Science, Kyoto University, Kyoto, Japan

69. Institut de Ciències de l'Espai (IEEE-CSIC), Campus UAB, 08193 Barcelona, Spain

70. Institució Catalana de Recerca i Estudis Avançats (ICREA), Barcelona, Spain

71. 3-34-1 Nishi-Ikebukuro,Toshima-ku, Tokyo 171-8501, Japan

72. Department of Physics, Center for Cosmology and Astro-Particle Physics, The Ohio State University, Columbus, OH 43210, USA

73. Praxis Inc., Alexandria, VA 22303, resident at Naval Research Laboratory, Washington, DC 20375, USA

74. Durtal Observatory, 6 Rue des Glycines, F-49430 Durtal, France

75. Dipartimento di Fisica "Enrico Fermi", Università di Pisa, Pisa I-56127, Italy

76. Hamburger Sternwarte, Gojenbergsweg 112, 21029, Hamburg, Germany

77. Ammon, ID 83401, USA

78. INAF Osservatorio Astronomico di Trieste, Via G. B. Tiepolo 11, 34131 Trieste, Italy

79. American Astronomical Society, 2000 Florida Ave NW, Washington, DC 20009-1231, USA

80. School of Earth and Space Exploration, Arizona State University, PO Box 871404, Tempe, AZ 85287-1404, USA

81. 67 Rue Jacques Daviel, Rouen 76100, France